A Novel interaction of CLN3 with nonmuscle myosin-IIB and defects in cell motility of *Cln3*^{-/-} cells

Amanda L Getty[1,4], **Jared W Benedict**[1], and **David A Pearce**[1,2,3,4,5,*]

[1]Center for Neural Development and Disease, Aab Institute of Biomedical Sciences, University of Rochester School of Medicine and Dentistry, Rochester, New York 14642

[2]Department of Biochemistry, University of Rochester School of Medicine and Dentistry, Rochester, New York 14642

[3]Department of Neurology, University of Rochester School of Medicine and Dentistry, Rochester, New York 14642

[4]Sanford Children's Health Research Center, Sanford Research USD, Sanford School of Medicine of the University of South Dakota, Sioux Falls, South Dakota 57117

[5]Department of Pediatrics, Sanford School of Medicine of the University of South Dakota, Sioux Falls, South Dakota 57117

Abstract

Juvenile neuronal ceroid lipofuscinosis (JNCL) is a pediatric lysosomal storage disorder characterized by accumulation of autofluorescent storage material and neurodegeneration, which result from mutations in CLN3. The function of CLN3, a lysosomal membrane protein, is currently unknown. We report CLN3 interacts with cytoskeleton-associated nonmuscle myosin-IIB. Both CLN3 and myosin-IIB are ubiquitously expressed, yet mutations in either produce dramatic consequences in the CNS such as neurodegeneration in JNCL patients and *Cln3*$^{-/-}$ mouse models, or developmental deficiencies in *Myh10*$^{-/-}$ mice, respectively. A scratch assay revealed a migration defect associated with *Cln3*$^{-/-}$ cells. Inhibition of nonmuscle myosin-II with blebbistatin in WT cells resulted in a phenotype that mimics the *Cln3*$^{-/-}$ migration defect. Moreover, inhibiting lysosome function by treating cells with chloroquine exacerbated the migration defect in *Cln3*$^{-/-}$. *Cln3*$^{-/-}$ cells traversing a transwell filter under gradient trophic factor conditions displayed altered migration, further linking lysosomal function and cell migration. The myosin-IIB distribution in *Cln3*$^{-/-}$ cells is elongated, indicating a cytoskeleton defect caused by the loss of CLN3. In summary, cells lacking CLN3 have defects that suggest altered myosin-IIB

*Correspondence should be addressed to: David A Pearce, Sanford Children's Health Research Center, Sanford Research USD, Sanford School of Medicine of the University of South Dakota, 1305 W. 18th St, PO Box 5039, Sioux Falls, SD 57117-5039. PearceD@sanfordhealth.org; Telephone: 605-312-6004; Fax: 605-328-0401.

Publisher's Disclaimer: This is a PDF file of an unedited manuscript that has been accepted for publication. As a service to our customers we are providing this early version of the manuscript. The manuscript will undergo copyediting, typesetting, and review of the resulting proof before it is published in its final citable form. Please note that during the production process errors may be discovered which could affect the content, and all legal disclaimers that apply to the journal pertain.

CONFLICT OF INTEREST

The authors have no conflicts of interest to declare.

activity, supporting a functional and physical interaction between CLN3 and myosin-IIB. We propose the migration defect in *Cln3$^{-/-}$* results, in part, from the loss of the CLN3-myosin-IIB interaction.

Keywords

Batten disease; motility; scratch assay; neurodegeneration

INTRODUCTION

Juvenile neuronal ceroid lipofuscinosis (JNCL) is a lysosomal storage disorder resulting in early-onset neurodegeneration in children. Patients present with blindness between ages 5–9 preceding progressive seizures, cognitive and motor decline, schizophrenic and Parkinsonian symptoms, and eventual premature death in the second or third decade of life [1]. NCL's are the most common pediatric neurodegenerative diseases in the world (1:12,500 live births), and JNCL is the most prevalent, resulting from autosomal recessively inherited mutations in *CLN3* [2–3]. Characteristic accumulation of autofluorescent storage material in all tissues occurs; however, pathology affects the central nervous system. Studies in *Cln3$^{-/-}$* mice have revealed that neuronal cell death, astrocytosis and gliosis are all evident [1, 4–7]. Defining the primary function of the CLN3 protein is fundamental to developing treatments for JNCL patients.

Numerous studies have examined consequences of the loss of CLN3. In patient cells, disruptions in pH homeostasis, amino acid transport and endocytosis have been described [8–9]. CLN3 is a transmembrane protein thought to reside in the lysosome [10], but has been localized to Golgi, endosomes, and synaptic compartments [11]. In order to determine the primary function of CLN3, identifying protein interactors is crucial. Several proteins associated with the cell periphery physically interact with CLN3 including: calsenilin, a neuronal calcium-binding protein [12], the fodrin-Na$^+$-K$^+$-ATPase complex [13], and transient interactions with Hook1, a microtubule-associated protein [8]. Additionally, CLN3 interacts with SBDS [14], a protein involved in ribosomal biogenesis and maturation. Therefore, CLN3 has multiple interacting partners; clues to the function of CLN3 may be elucidated by fully understanding the complex CLN3 interaction network.

To further identify interactions of CLN3 in the brain, where JNCL patients are severely affected, peptide fragments of CLN3 were screened against a human fetal brain library using a cytoplasmic yeast-2-hybrid technique (Stratagene's Cytotrap). The C-terminal fragment of CLN3 was found to interact with non-muscle myosin-IIB, an actin-binding motor protein. Myosin-IIB has important functions in cytokinesis, maintenance of cell polarity, and formation of focal contacts [15–19]. A myosin-IIB interaction with an NCL protein is not the first association of a nonmuscle myosin-II with disease. Nonmuscle myosin-IIA (*MYH9*) mutations cause a family of autosomal-dominant macrothrombocytopenias: May-Hegglin anomaly, Sebastian syndrome, Fechtner syndrome, and Epstein syndrome [20]. Ablation of myosin-IIB in mice is embryonic lethal, and myosin-IIB (*MYH10*) mutations are thought to be embryonic lethal in humans, as well; however, myosin-IIB function has been associated

with the pathogenesis of spinocerebellar ataxia type 6 (SCA6) through associations of myosin-IIB and Cav2.1 calcium channel polyglutamate tracts [21]. In the central nervous system (CNS), myosin-IIB function has been associated with dendritic spine morphology [22], cell guidance [16], growth cone motility in neurites [23], presynaptic vesicle trafficking [24], among others (reviewed, [25]). We have shown previously that inhibition of nonmuscle myosin-II by blebbistatin treatment accelerated accumulation autofluorescent storage material in lymphoblasts [26], implicating alterations in nonmuscle myosin-II function in NCL pathways. Therefore, the function of the myosin-IIB-CLN3 interaction may have consequences for CLN3 loss in the cell, and offer clues as to the primary function of CLN3.

In myosin-IIB-ablated cells, there is a marked defect in cell migration over a poly-d-lysine coated substrate [16]. The loss of myosin-IIB causes changes in polarized cell morphology to transient, disorganized lamellipodia, which are thought to contribute to improper cell guidance and polarity [16, 18]. In this study, a traditional cell migration scratch assay was performed in *Cln3*$^{-/-}$ mouse embryonic fibroblasts and revealed a deficiency in migration, which may be in part due to the loss of the myosin-IIB-CLN3 interaction in these cells. We did not detect a defect in proliferation or cell viability in *Cln3*$^{-/-}$; thus, it seems the myosin-IIB-CLN3 interaction may be important for cell migration and morphology. The loss of the myosin-IIB-CLN3 interaction may be contributing to cellular defects that manifest in JNCL.

Material and methods

Yeast Two Hybrid

Stratagene's Cytotrap Yeast 2-Hybrid (Y2H) system (Stratagene, La Jolla, CA) was used to screen for CLN3 interactions. The C-terminus of CLN3 (amino acids 387–438; Genbank accession number NM_001042432) was cloned into the pSos vector, which will produce a fusion protein of the CLN3 peptide with the human Sos protein (amino acids 1–1067). The hSos-CLN3 C-terminus fusion protein was screened against a human fetal brain cDNA library expressed by the pMyr vector, which adds a myristylation moiety to library proteins. The Y2H screen was performed as previously published, assaying for suppression of the *cdc25h* yeast strain temperature-sensitive phenotype at 37°C in the presence of galactose [14, 27–29]. Potential interactors were re-screened to validate positive candidates, and interactors were sequenced using primers specific for the pMyr vector. Non-muscle myosin-IIB (GenBank accession: NM_005964 XM_290747; Swiss-Prot accession number P35580.3) sequence (amino acids 585–1010) was identified to interact with the C-terminus of CLN3.

Antibodies

The following antibodies were used for immunohistochemistry, immunocytochemistry, immunoprecipitation, and immunoblotting experiments: anti-myosin-IIB (CMII23, Iowa Developmental Studies Hybridoma Bank), anti-myosin-IIA (Covance, Emeryville, CA), anti-Myc (Cell Signaling, Danvers, MA), LAMP1 (1D4B, Iowa Hybridoma Bank), anti-β-Actin (Sigma, St. Louis MO), anti-calbindin (Sigma, St Louis, MO), and anti-β-catenin (BD

Biosciences, San Jose, CA). Cell and tissue samples were subsequently incubated with appropriate AlexaFluor secondary antibodies (Molecular Probes, Inc, Eugene, OR).

Generation of primary mouse embryonic fibroblast (MEF) cultures

All animals were housed under identical conditions and all procedures followed the guidelines of both the NIH and the University of Rochester Animal Care and Use Committee. Timed pregnant WT (129Sv/J) and *Cln3*$^{-/-}$ (on 129Sv/J background) [30–31] mice were euthanized and embryos were harvested at embryonic day 17.5 (E17.5). Fibroblasts were prepared as described previously [16] using standard techniques. Cells were maintained in complete DMEM media, which includes 10% FBS, non-essential amino acids, penicillin/streptomycin, and L-glutamine (Gibco, Invitrogen, Grand Island, NY). No MEF cultures were used for migration experiments after 5 passages, or approximately 2 weeks in culture.

Immunoprecipitation and Immunoblotting

CLN3 was subcloned into the pCMV multiple cloning site of the pBudCE4.0 vector (Invitrogen Carlsbad, CA), which expresses the protein with a small C-terminal myc tag. The CLN3-pBudCE4.0 construct or empty pBudCE4.0 was transfected into NIH/3T3 fibroblasts using Lipofectamine 2000 (Invitrogen, Carlsbad, CA). The protein was expressed for 36 hours, and extracted using non-denaturing lysis buffer (50 mM Tris-Cl, pH 7.5, 300 mM NaCl, 5 mM EDTA, 1% Triton X-100). Anti-myc antibody was added to equal amounts (~1 mg cell lysate protein) of CLN3 or empty vector transfected pre-cleared cell lysate followed by incubation with protein A-agarose beads (Sigma, St Louis, MO). Beads were washed with a non-denaturing wash buffer (50 mM Tris-Cl, pH 7.5, 300 mM NaCl, 5 mM EDTA, 0.01% Triton X-100). The final pellet was resuspended in Laemmli loading buffer and boiled. Samples from the immunoprecipitation and lysate (~30 μg) were analyzed by Western blot for myosin-IIB and LAMP1. Densitometry analysis was performed using an AlphaImager v5.5 (Imgen Technologies, Alexandria, VA) and the mean pixel density of each protein of interest was normalized to the mean pixel density of β-actin.

Immunofluorescence

Colocalization in NIH/3T3 fibroblasts expressing CLN3-Myc was prepared as previously described [14] and images were acquired at 100× using an inverted Olympus IX81 and Olympus FluoView™ FV1000 confocal microscope (Olympus America, Inc; Center Valley, PA) and the Olympus FluoView™ Ver. 1.7c software. MEF scratches were processed similarly and images were acquired using an Olympus BX61 microscope (Olympus America, Inc; Center Valley, PA) and images were captured at 20× or 40× with a CoolSNAP HQ camera (Roper Scientific GmbH, Germany) and IP-Lab4 software (BD Biosciences, San Jose, CA) or a Nikon Eclipse 90i microscope (Nikon instruments, Inc., Melville, NY) with a CoolSNAP HQ camera (Roper Scientific GmbH, Germany) and NIS-Elements. For immunological examination of WT and *Cln3*$^{-/-}$ mouse cerebellum, sections and protein homogenates were prepared as previously described [7, 32–33]. Measurements of myosin-IIB area, length, and width were performed using NIS-Elements Software (Nikon Instruments Inc., Melville, NY). At least 5 randomly selected fields of view from each of at

least 5 scratch assays were acquired for morphology measurements, with a total number of cells measured between 100–120 cells per genotype.

Cell Migration Assays

Scratch Assay—MEF cells were placed on poly-D-lysine coated 12-well plates (Costar Corning, Inc, Corning, NY) at a cell density of 2×10^5 cells/well in complete media. At time 0, a 200-μL pipette tip was used to perform scratches in the confluent monolayer. The media was replaced with complete media or complete media including the following treatments: 10μg/mL chloroquine (Sigma), or 10μM or 50μM blebbistatin (Sigma). At specified time points, images were acquired of scratches, using the marked plate bottom for orientation, with an Olympus 1X71 microscope and Olympus DP72 camera and DPController Software (Olympus America, Inc; Center Valley, PA). Measurements of scratch distance were completed using ImageJ (NIH, http://rsb.info.nih.gov/ij/, version 1997–2009) by measuring the difference between the length of the initial scratch and the length of the scratch at the specified time point, divided by 2 to account for two sides of the scratch closing simultaneously. Eight measurements were completed for each scratch at each time point. Four scratches were used for each treatment condition and experiment, and the experiments were repeated with three separate MEF preparations. Rates of scratch closure were calculated as the distance (μm) MEFs traveled relative to the initial scratch, divided by the time.

Transwell Assay—MEFs were washed three times with serum-free media and seeded on a 3.0 μm Fluoroblok™ transfilter (BD Biosciences, Falcon, San Jose, CA) in 500 μL of serum-free media and then placed within complete medium and incubated for 24 hours. The transfilter was then prepared for immunofluorescence using DAPI to stain nuclei. The number of fluorescent nuclei per 20× field of 5 views on the bottom of a transfilter was counted. All experiments were completed in triplicate both in technical and biological replicates.

Statistical significance was determined by 2-way ANOVA, Bonferroni's Post-Hoc tests, and Student's T-test using GraphPad Prism (San Diego, CA).

Cell Viability and Proliferation Assays

BrdU incorporation was performed as previously described [7]; however in brief, cells grown on coverslips and subjected to the scratch assay were pulsed for two hours with 10μM BrdU (Sigma), then washed with ice cold TBS followed by fixation with 4% paraformaldehyde/4% sucrose phosphate buffer (pH 7.5). Cells were washed with TBS with 0.1% Triton X-100 and incubated with 1M HCl, followed by two washes with 0.1M borate buffer (pH 8.5). Cells were then treated with Blotto (4% nonfat dried milk, TBS, 0.1% Triton X100). The anti-BrdU antibody (BD Pharmingen) was incubated overnight and secondary AlexaFluor antibodies and DAPI nuclear stain (both from Invitrogen) were used for visualization. Coverslips were mounted with ProLong Anti-Fade mounting medium (Molecular Probes, Invitrogen). Five randomly selected fields of view, using the DAPI (405) channel only, were acquired for each coverslip examined, with at least 3 coverslips used per condition, and at least two different MEF culture preparations, for a total N = 5–8 per

condition. BrdU incorporation measured prior to the scratch assay was performed approximately 16 hours after plating. MTT assay was performed as previously described [34]. Statistical significance was determined by Student's T-test, 2-way ANOVA and Bonferroni's Post-Hoc tests using GraphPad Prism (San Diego, CA).

RESULTS and DISCUSSION

CLN3 interacts with the cytoskeleton associated protein: non-muscle myosin-IIB

Yeast-2-hyrid (Y2H) has been used previously to identify interactions with CLN3 [12–14, 29]. The CytoTrap Y2H method (Stratagene) uses a *cdc25h* yeast strain that is temperature sensitive at 37°C due to a mutation in the *CDC25* gene, which is homologous to human Sos protein. hSos/cdc25 is a guanine nucleotide exchange factor (GEF) that is responsible for activation of the Ras pathway [35]. Ras is located at the plasma membrane, and translocation of hSos/cdc25 to the plasma membrane facilitates GDP-GTP exchange, promoting active Ras-GTP to propagate the MAPK/ERK pathway. Activation of this pathway suppresses the temperature sensitivity of the *cdc25h* strain at 37°C. The advantage of this system is that interactions occur in the cytoplasm, associated with membranes, rather than in the nucleus as in traditional Y2H assays, which ensures a more native environment for cytosolic membrane proteins, such as CLN3. The predicted less hydrophobic fragments of CLN3, based on the six-membrane domain topology predicted by [36–37] (Supplemental Figure 1a,c), were fused with hSos and co-transformed into the *cdc25h* yeast strain with a human fetal brain library that was expressed with an added myristylation moiety to anchor library proteins in membranes; both genes were driven by a galactose-inducible promoter, as has been previously described [14]. A positive interaction between the C-terminus of CLN3 and the myristylated library protein at the membrane would allow for Ras activation and suppression of the temperature-sensitive phenotype at 37°C in the presence of galactose.

Using the Cytotrap Y2H system, the hydrophilic peptides of CLN3 were screened against a human fetal brain cDNA library. This assay revealed several potential interactors with CLN3, including an interaction with Shwachman-Bodian-Diamond (SBDS) protein [14] and a novel interaction between the C-terminus of CLN3 (amino acids 387–438) and non-muscle myosin heavy chain-IIB (amino acids 585–1010; *Myh10*, hereafter referred to as myosin-IIB) (Figure 1a). Myosin-IIB is an actin-binding cytoskeletal protein that is involved in cell shape, cell motility and cytokinesis [16–18, 25, 38]. The region of myosin-IIB that was identified in the Y2H screen spans the motor region, the regulatory myosin light chain binding region, and part of the coiled-coil domain of the protein (Supplemental figure 1b, d).

Suitable CLN3 antibodies for detecting endogenous CLN3 are unavailable, so a small myc tag was added to CLN3 for subsequent experiments. Co-immunoprecipitation using the myc-tagged CLN3 showed an interaction with endogenous myosin-IIB (Figure 1b). Protein expression in NIH/3T3 fibroblasts was confirmed by immunoblotting protein lysates (Figure 1c). CLN3 did not interact with the myosin-IIA isoform by co-immunoprecipitation (Figure 1d), which is further supported by the lack of detection of myosin-IIA in the Y2H screen. The fragment of myosin-IIB that was found by Y2H contains several unique amino acid sequences (for example in the tail region of myosin-IIB amino acids 865–895), and such patches may provide isoform-specificity of this interaction. To further validate this myosin-

IIB-CLN3 interaction, we immunoprecipitated and assayed for LAMP1, a lysosomal membrane protein in the same compartment with CLN3, and LAMP1 did not co-immunoprecipitate with CLN3 (Figure 1e) or myosin-IIB (data not shown). Transfected NIH/3T3 cells stained with anti-myc and anti-myosin-IIB antibodies confirmed that the two proteins co-localized in distinct puncta indicating that these proteins have the opportunity to interact in cells (Figure 1f). Due to the relative high abundance of myosin-IIB to CLN3 in the cell, it makes sense that vesicular CLN3 interacts with a portion of the myosin-IIB pool either within myosin-IIB oligmeric structures, or inactive dimmers [39]. Taken together, these data demonstrate that myosin-IIB interacts with CLN3.

Cln3−/− mouse embryonic fibroblasts exhibit a cell migration defect

A fibroblast scratch assay is a classic measure for cell migration and myosin-II function [16, 40]. The scratch assay involves mechanically disrupting a confluent monolayer and observing "closure of the scratch" as cells migrate. A defect in *Cln3*−/− fibroblast migration could provide a functional link between these two proteins. Cultures of primary mouse embryonic fibroblasts (MEF) were prepared from WT and *Cln3*−/− mice and subjected to a scratch assay (Figure 2a). Following disruption of the confluent monolayer, WT cells migrated into the scratch and closed the gap within 24 hours; however, *Cln3*−/− cells exhibited a delay in migration and did not close the scratch until approximately 36 hours (Figure 2b). The rate of scratch closure is significantly decreased in the absence of CLN3 (Figure 2c). A migration defect phenotype, as seen here in *Cln3*−/− cells, also exists in myosin-IIB siRNA-treated cells [40]. Myosin-IIB depleted fibroblasts close the scratch despite significant delays in migration [16], and *Cln3*−/− fibroblasts also close the scratch at a delayed rate relative to WT. There are several explanations for the mechanism of this migratory defect resulting from CLN3 deficiency, and these include: defects in cellular proliferation or metabolic status, altered protein localization, insufficient cell adhesion, or deficient cell motility, all could potentially link myosin-IIB function with CLN3.

One factor that could contribute to deficient *Cln3*−/− fibroblast migration could be a decrease in cell proliferation into the scratch [41]. In order to determine the viability of *Cln3*−/− cells to ensure the cell motility defect was not simply due to deficiency in cell integrity, the proliferative status of MEFs was examined by incorporation of 5-bromo-2-deoxyuridine (BrdU). BrdU is a thymidine analog that is inserted into newly synthesized DNA, which can then be labeled with BrdU-specific antibodies to highlight actively proliferating cells [42]. The number of DAPI nuclei, representative of the number of cells (Figure 3a), and the ratio of BrdU+ cells to the total number of cells was measured at the leading edge of the scratch (Figure 3b; Supplemental Figure 2e). The ratio of BrdU+ *Cln3*−/− cells is significantly higher than WT. If a difference in proliferation was contributing to the scratch assay phenotype, then WT cells would likely have a higher ratio of BrdU+ cells, but this is not the case.

In order to determine if the difference between BrdU+ incorporation in WT and *Cln3*−/− cells is specific to the leading edge of the scratch, confluent areas were examined away from the scratch (Supplemental Figure 2a,b). There is a higher ratio of BrdU+ *Cln3*−/− cells than WT, indicating that in these primary MEF cultures, there are more proliferating *Cln3*−/− cells. Both genotypes are plated at the same density and are confluent before the scratch;

additionally, BrdU incorporation prior to the scratch assay indicates no difference between the genotypes (Supplemental Fig. 2c,d). Therefore, proliferation rate of $Cln3^{-/-}$ cells must increase during the course of the scratch assay, throughout the entire confluent culture.

Secondarily, the MTT assay provides a measure of cell viability by determining the level of succinate dehydrogenase activity within respiring cells. By MTT assay, there was no difference in cell viability between WT and $Cln3^{-/-}$ fibroblasts at the plating densities used for the scratch assay before (Supplemental Figure 3a) or following the scratch assay (Supplemental Figure 3c). In summary, the migration defect of $Cln3^{-/-}$ cells is not due to differences in viability or cellular metabolism in $Cln3^{-/-}$ MEF cells, as measured by MTT assay. It is not likely that a difference in cellular proliferation between WT and $Cln3^{-/-}$, as indicated by BrdU incorporation, contributes to the scratch assay phenotype that we observe.

In order to determine the contribution of the loss of the CLN3-myosin-IIB interaction to the scratch assay phenotype, we treated MEF cells with a small molecule inhibitor of the ATPase activity of non-muscle myosin-II, blebbistatin [43] (Figure 4a,c). Blebbistatin will inhibit all three isoforms of nonmuscle myosin-II, with IC_{50} of 5.1 μM for myosin-IIA and 1.8 μM for myosin-IIB [43]; however, only the myosin-IIB isoform has been shown to interact with CLN3. Any differences in phenotypes between WT and $Cln3^{-/-}$ cells associated to myosin-II function, for instance, due to myosin-II inhibition with blebbistatin, may be due to a loss of this functional interaction in $Cln3^{-/-}$ cells. As expected, blebbistatin inhibits the distance and rate of WT MEF cell migration into the scratch (Figure 4d). Treating MEF cells with blebbistatin delayed WT MEF cell movement into the scratch in a manner that mimics the $Cln3^{-/-}$ MEF cell phenotype (Figure 4c,d), which suggests that the defect in $Cln3^{-/-}$ involves myosin-IIB function. Most strikingly, the phenotype in $Cln3^{-/-}$ cells was unchanged by myosin-IIB inhibition using blebbistatin treatment (Figure 4e), indicating that the defect in migration was already present in cells with CLN3 deficiency. Thus, the rate of scratch closure in WT MEF cells is decreased by blebbistatin treatment, but $Cln3^{-/-}$ cells remain unchanged (Figure 4f). Combined with previous observations that blebbistatin treatment increases accumulation of autofluorescent storage material in lymphoblasts [26], myosin-IIB appears to be involved in CLN3 pathways, which will also be disrupted in JNCL cells.

JNCL is characterized as a lysosomal storage disorder due to the distinctive accumulation of autofluorescent storage material in the lysosomes of JNCL cells. CLN3 has been found to localize to the lysosomes, endosomes, and acidic vesicles of the synaptic compartment [11], and alterations in lysosomal function have been found with CLN3 loss [44–46]. Since lysosomal function has not previously been implicated in cell migration phenotypes, we disrupted lysosomal function with chloroquine to determine the effect on cell motility. Chloroquine is a small molecule that is sequestered into lysosome and endosomes, where its presence increases the pH of these vesicles. The increase in pH disrupts the integrity of the lysosomal compartment and thus prevents resident proteases and enzymes function [47–48]. If CLN3 is a resident lysosomal protein that is involved in acidic vesicle homeostasis, then in its absence a further insult to the lysosome may be unrecoverable for the cell. During chloroquine treatment, the distance of WT and $Cln3^{-/-}$ MEF migration was decreased (Figure 5), and the difference in migration rate between WT and $Cln3^{-/-}$ was maintained

(Figure 5e). WT MEF cells overcame the delay in their migration, and eventually close the scratch (Figure 5b); however, *Cln3*$^{-/-}$ cells were incapable of overcoming this insult, and did not close the scratch (Figure 5a,c). The insult of CLN3 loss in the lysosome causes alterations in pH homeostasis [49–53], vesicle trafficking [45], endocytosis [8], and autophagy defects [54]. Chloroquine treatment further assaults the lysosome-endosome integrity by affecting many processes in the cell that involve acidic vesicle trafficking and lysosomal function [48]. Treatment of fibroblasts with chloroquine halts cell movement, but only when CLN3 dysfunction is also present. This significantly links the aforementioned functions of CLN3 to cell motility.

Incorporation of BrdU in cells treated with chloroquine or blebbistatin during the scratch assay was measured to determine the effect either of these drugs has on cell proliferation (Figure 6). Though the concentrations used for the scratch assay were optimized to minimize cell death (data not shown), decreases in BrdU incorporation were seen for chloroquine and blebbistatin treatments. Inhibition of nonmuscle myosin-II will cause a decrease in cytokinesis, and therefore a decrease in BrdU incorporation during myosin-II inhibition is not surprising [15]. Chloroquine treatment (at higher doses) has also been shown to decrease DNA synthesis indirectly [55]. Again, it is not likely that these changes in proliferation contribute to the scratch assay migration phenotype, but *Cln3*$^{-/-}$ cells are more sensitive to both chloroquine and blebbistatin treatments, as the number of BrdU^{+} cells decreases further in this genotype than WT.

Cln3$^{-/-}$ cell migration through a Boyden Chamber—The scratch assay measures migration is over a two-dimensional (2D) poly-d-lysine coated substrate, where cells are bathed in trophic factors and only seek to gain confluence. The movement of these cells is directed by different signals and stimuli than under gradient conditions that drive chemotaxis. It was shown previously that in a CNS-derived glioma cell line, myosin-IIB was involved in cell migration specifically during chemotaxis within a 3D substrate, such as in a matrigel invasion assay, but not in a traditional scratch assay [40]. This suggests a specific function of myosin-IIB under different kinds of migration and perhaps in different cell types. Therefore, we examined if the same migration defect seen in the fibroblast scratch assay exists in *Cln3*$^{-/-}$ MEF cells during 3-D migration assay. In the Boyden chamber assay, cells are plated above a barrier and sense a gradient of rich trophic factor support supplied in a lower chamber. The migratory signals that drive cells to seek these pores, contort cell bodies to drive processes through the pore and then to pull the nucleus through the pore, all require a more complicated set of signals and movements than over a 2D substrate [25, 40]. Therefore, WT and *Cln3*$^{-/-}$ cell migration was assayed through a 3.0μm porous filter under a gradient of fetal bovine serum (FBS). It was expected that due to the migration defect revealed by scratch assay, that *Cln3*$^{-/-}$ cells would have a similar defect in their ability to traverse a transfilter.

Surprisingly, after 24 hours of incubation, *Cln3*$^{-/-}$ cells traversed the filter more than WT cells (Figure 7a). A small pore size was required for selectivity between the genotypes (3.0μm), as a larger pore (8.0μm) filter did not prevent WT from traversing the filter (Figure 7b). This could indicate a difference cell morphology or size between WT and *Cln3*$^{-/-}$ cells that results from cytoskeletal abnormalities. The transwell assay was repeated with

chloroquine (Figure 7c), which abolished the movement of $Cln3^{-/-}$ cells, neither traversed the filter. This suggests that lysosome and acidic vesicle integrity is required for chemotaxis. Blebbistatin treatment also increased the movement of $Cln3^{-/-}$ cells through the filter, and also increased WT cells movement, as well (Figure 7d), which could reflect the elongated morphology that occurs when blebbistatin treatment causes collapse of the myosin-II associated cytoskeleton (Figure 4a). Taken together, the rates of WT and $Cln3^{-/-}$ migration into a scratched-2D substrate and the increased migration of $Cln3^{-/-}$ MEF chemotaxis in a gradient of trophic factors, suggests the involvement of lysosomes in cell motility.

$Cln3^{-/-}$ MEF cells are either particularly sensitive to the serum deprivation within the plating upper chamber, or to the trophic factor source signals within the lower chamber. Previous studies show no difference in JNCL patient fibroblasts in the uptake of biotin-transferrin; however when cells were preloaded with biotin-transferrin in the endosomes, transferrin recycling was slightly increased in JNCL fibroblasts [8]. Our results in fibroblasts could reflect a similar defect in endosomal trafficking or vesicle fusion post-endocytosis. There is evidence that CLN3 has been implicated in endocytosis defects in yeast [56], and $Cln3^{-/-}$ cells may require a higher concentration of growth factors in order to overcome the endocytosis defect. The $Cln3^{-/-}$ cell response to the gradient does not appear to be caused by alterations in cellular metabolism, as there was no difference by MTT assay (Supplemental Figure 3); however there may be a defect in $Cln3^{-/-}$ cell surface receptors recycling that affects their migratory behavior in a gradient of trophic factors. Myosin-IIB has been shown to have functions in exocytosis-based membrane repair and vesicle trafficking to the plasma membrane [57], and this could involve CLN3 through associations with the cytoskeleton and vesicle recycling at the plasma membrane.

Cln3$^{-/-}$ cells are elongated and have reduced cell area—In fibroblasts, non-muscle myosin-II is involved in lamellipodia extension at the leading edge, as well as focal adhesion localization and formation, nucleus movement towards the leading edge, and tail retraction for concerted movement [17–18]. If lysosomes or endosomes are involved in recycling of adherens junctions and focal adhesion complexes during cell movement, it is possible that the myosin-IIB-CLN3 interaction is involved in the direction and coordination of this process, which would be deregulated in its absence. Therefore, migrating fibroblasts were stained with an anti-myosin-IIB. There are alterations in myosin-IIB staining, towards the leading cortical side of $Cln3^{-/-}$ cells (Figure 8). Strikingly, $Cln3^{-/-}$ cells have an elongated morphology in which the lagging tail seems to be deficient in retraction (Figure 8).

In order to quantify change in fibroblast morphology in $Cln3^{-/-}$ cells, fibroblasts migrating into the scratch were stained with anti-myosin-IIB antibodies and measured for area, length and width (for representative images, Supplemental Figure 5). The area of myosin-IIB staining in each cell is used here as a measure of cell area, though it is possible that the cell area extends beyond the actin-myosin cytoskeleton. These measurements revealed that $Cln3^{-/-}$ cells are longer (Figure 9a) and narrower (Figure 9b) than WT, and the ratio of the length to width indicates that $Cln3^{-/-}$ cells have a quantifiable elongated morphology (Figure 9c). Further, the area of myosin-IIB distribution in $Cln3^{-/-}$ cells is significantly smaller (Figure 9d). If a "skinny cell" is defined as a cell with a high ratio of length to width (greater than 3.0) and a small area (less than $1000\mu m^2$), then in a 20x field of view there is a

greater number of "skinny cells" in $Cln3^{-/-}$ fibroblasts at the leading edge of a scratch than WT (Figure 9e,f). Therefore, the loss of CLN3 affects the myosin-IIB distribution or the myosin-associated cytoskeleton architecture in these cells. This effect could be directly related to CLN3 function, or could be a result of lysosomal dysfunction that is caused by CLN3 loss.

Alternatively, the elongated appearance of $Cln3^{-/-}$ fibroblasts could be explained by changes in adherens junction distribution within cells, which could affect cell adhesion and organization in the confluent monolayer. In WT cells, adherens junction complexes, illustrated by punctate β-catenin distribution, are concentrated at the cell periphery; whereas in $Cln3^{-/-}$ cells there seems to be a more random distribution of these complexes, which may indicate a disordered distribution of important adhesions and signaling (Figure 10). In aortic endothelial cells there is an asymmetric distribution of isoforms of nonmuscle myosin-II, with myosin-IIB concentrated at the tailing edge [58]; also myosin-IIB knockdown during myoblast fusion decreased tail retraction [38]. Therefore, the cell morphology changes that are seen in $Cln3^{-/-}$ MEF cells mimic morphology changes when myosin-IIB function is altered.

The cell morphology of WT fibroblasts during chloroquine treatment was observed to be markedly elongated and contracted (Figure 5, 11), and quantification of the myosin-IIB area, length, and width during this treatment (Figure 11a–d) indicated that there was in fact a decrease in WT cell width and area with chloroquine treatment. In fact, chloroquine treatment caused an increase in the number of skinny cells observed at the leading edge, similar to $Cln3^{-/-}$ cells (Figure 11e). Myosin-IIB distribution within the elongated cells during chloroquine treatment in WT and $Cln3^{-/-}$ fibroblasts looks very similar (Figure 11f). However, the adherens junctions or β-catenin punctate staining is no longer at the cell periphery, but mostly perinuclear and throughout the cells of both genotypes (Figure 11f). Normally, a decrease in cell-cell adhesion would predict increased migration as cells are liberated towards the open surface; however, a decrease in migration was seen in the scratch assay during chloroquine treatment. This suggests the lysosomal/endosomal network, and CLN3, are important in the integrity of adherens junctions and cell motility.

Blebbistatin causes dramatic and reversible changes in cell morphology, as previously described in other cell types [59], and observed here for myosin-IIB and adhesion complexes (β-catenin) (Figure 12 b, c, h, i). Inhibition of nonmuscle myosin-II causes a loss of organized adhesion complex formation, loss of cell polarity and directionality, and disorganization of protrusions [39]. If $Cln3^{-/-}$ fibroblasts exhibited differences in myosin-IIB distribution or cell morphology during blebbistatin treatment, it could highlight a specific function for CLN3 in one of these particular functions of myosin-IIB. However, both genotypes changed similarly under blebbistatin treated-conditions (Figure 12). Overall, there did not seem to be any gross difference in the distribution of adherens junctions, indicated by β-catenin, or actin-myosin associated cytoskeleton by myosin-IIB staining, between WT and $Cln3^{-/-}$ fibroblasts under high (50μM) or low (10μM) blebbistatin conditions. However, while WT MEF cells, stained with myosin-IIB antibodies, are totally collapsed under low (10μM) blebbistatin (Figure 12b), the myosin-IIB staining in $Cln3^{-/-}$ MEF cells does not fully collapse until higher (50μM) blebbistatin concentrations (Figure

12h and 12i). All of the punctate β-catenin staining is diffuse with blebbistatin treatment (Figure 12d–f; j–l). Individual cell morphology quantification measurements were not possible during the blebbistatin treatment as the cell boundaries are indistinguishable in the contracted cell morphology that results from myosin-II inhibition.

In summary, the actin-myosin cytoskeleton and cellular morphology of *Cln3*$^{-/-}$ fibroblasts is altered. This further supports an interaction between lysosomal function and the cytoskeleton, perhaps mediated in part through a direct physical interaction between myosin-IIB and CLN3, which is lost in *Cln3*$^{-/-}$ cells. It is most likely that these alterations in the cytoskeleton, that cause *Cln3*$^{-/-}$ cells to take on an elongated shape, permit the accelerated movement through the porous filter, and could in fact be the cause of the Boyden chamber assay phenotype.

Myosin-IIB expression and distribution in *Cln3*$^{-/-}$ mouse cerebellum

Ultimately, mutations in CLN3 cause JNCL, a disease that affects the central nervous system. Myosin-IIB has been shown to be particularly important in the brain, where it is the major non-muscle myosin-II isoform expressed [60–63]. A mutation within the motor domain of myosin-IIB in mice showed abnormal cerebellar foliation and layer formation, along with ataxia and motor coordination defects [64], motor coordination deficits are also observed in *Cln3*$^{-/-}$ mice by accelerating rotorod [7]. Therefore, the cerebellum may be a tissue where the CLN3-myosin-IIB interaction could be important. Therefore, Myosin-IIB distribution and expression was examined in the cerebellum of *Cln3*$^{-/-}$ mice. *In situ* hybridization shows both *Cln3* and *Myh10 (myosin-IIB)* transcripts present in multiple classes of cells within the adult cerebellum, including granule cells, Purkinje cells, and interneurons within the molecular cell layer (http://www.brain-map.org). Total myosin-IIB protein (Figure 13a) and mRNA levels (data not shown) were not different between the genotypes in any region of the cerebellum. Immunolabeling for calbindin, a marker of Purkinje cells and for myosin-IIB showed no major difference in the cellular distribution of myosin-IIB (Figure 13b); although, a subpopulation of Purkinje neurons displayed abnormal punctate myosin-IIB staining in *Cln3*$^{-/-}$. It is possible that alterations in myosin-IIB distribution due to loss of the myosin-IIB-CLN3 interaction occur at levels below the detection limit of this assay, or occur under specific time points of development not examined here. However, our previous observations in the cerebellum of *Cln3*$^{-/-}$ mice could indicate deficiencies in neuronal migration or morpohology.

We recently reported that *Cln3*$^{-/-}$ mice have a decreased number of cells found in the deep cerebellar nuclei, Bergmann glia activation, misorientation of Purkinje cells, and an increased Purkinje cell spine number [7]. As myosin-IIB is required for cell polarity, adhesion, and migration, which are all vital for neuronal cell function and integrity [39], it is possible that loss of the interaction with CLN3 in these cells contributes to the dysfunction that causes these phenotypes. An increase in Purkinje cell spine number is opposite of what is observed in the B2-ablated myosin-IIB mice, where a decrease in Purkinje cell spine number is found [7, 65]. Alterations in spine morphology and number have been linked with myosin-IIB [22] and separately with ESCRT complexes, proteins involved in endosomal trafficking and membrane fusion events, [66] it is possible that the differences in dendritic

spine number in *Cln3*$^{-/-}$ Purkinje cells could be due to a loss of the interaction of CLN3 and myosin-IIB indirectly. There is biochemical evidence that myosin-IIB [67] and CLN3 [68] have been found associated with detergent-resistant membranes, and that these structures are required for dendritic spine morphology [69]. One might speculate that CLN3 functions in the recycling or down-regulation of myosin-IIB at distinct microdomains in neurons, such that a loss of CLN3 would appear to lead to an increased activity of myosin-IIB or an increase number of spines. Ablation of a myosin-IIB splice variant, which is expressed exclusively in the Purkinje cells and Bergmann glia of the cerebellum, results in abnormal Purkinje cell spine number, misshapen and misplaced Purkinje cells, thinning of the internal granule cell layer and impaired balance on the rotarod [65]. The loss of the CLN3-myosin-IIB interaction in *Cln3*$^{-/-}$ mice could contribute to the similar phenotypes or cellular disruptions seen in myosin-IIB mutant mice, since it is likely that the CLN3-myosin-IIB interaction is disrupted in both mice. What is clear, is that *Cln3*$^{-/-}$ mice show alterations in cell morphology in the cerebellum in Purkinje neurons, which may be analogous to changes we see in fibroblasts, but manifest differently due to the different cell types. Subsequent publications will examine the neuronal phenotypes directly.

CONCLUSIONS

Here, we have demonstrated a migration defect in *Cln3*$^{-/-}$ cells associated with a novel interaction of myosin-IIB and CLN3. The migration defect is not likely due to differences in proliferation or viability of *Cln3*$^{-/-}$ cells. Localization of myosin-IIB seems changed in *Cln3*$^{-/-}$ cells, as *Cln3*$^{-/-}$ fibroblasts exhibit an elongated morphology and collapsed myosin-IIB architecture. This elongated morphology could explain why more *Cln3*$^{-/-}$ cells traversed the Boyden chamber in a gradient of trophic factors, as "skinnier" *Cln3*$^{-/-}$ cells would be able to squeeze through pores in the transfilter easier than WT. Chloroquine treatment decreased the movement of *Cln3*$^{-/-}$ cells in the Boyden transwell assay, however, again reflecting the interdependence of lysosomal function and cell motility. The loss of the lysosomal protein, CLN3, causes a accumulation of autofluorescent storage material resulting in a lysosomal storage disorder and perturbations in lysosomal enzymes [70–71], such as reduction in cathepsin B activity [45]. Therefore it is possible that in *Cln3*$^{-/-}$ fibroblasts, the integrity of lysosomes is fragile and an additional insult, such as chloroquine treatment, causes dysfunction that cannot be compensated for in order for cells to be motile and maintain normal morphology. So, *Cln3*$^{-/-}$ cells are elongated and traverse the filter under trophic factor deprivation conditions. However, when chloroquine treatment challenges the cells beyond their capability to compensate, they are unable to traverse the filter, and probably are unable to respond to the gradient of trophic factors due to the loss of the acidic vesicle integrity. In a recent report, CLN3 was shown to be osmoregulated and highly expressed in the renal inner medulla, as well as other epithelial cell types, and evidence suggests a role for CLN3 in maintenance of cell volume [72]. Our observations of elongated *Cln3*$^{-/-}$ fibroblast morphology support this study. Finally, if cell adhesion defects played a role in either migration assay, then changes in adherens junction distribution would be expected, however adherens junctions (β-catenin staining) were not grossly altered by the absence of CLN3. Thus, it seems likely that the defect seen in *Cln3*$^{-/-}$ cell migration into the scratch assay is directly due to defects in cell motility and cytoskeleton.

Defining the function of CLN3 in cells is critical to the development of treatments for JNCL. Currently, several functions for CLN3 have been proposed based on phenotypes observed during the loss of CLN3, including this study. Disruptions in lipid metabolism or trafficking of lipids [73–74] or vesicles and endocytosis recycling [8], amino acid transport [75–76], and pH homeostasis [77–78], as well as resistance to apoptosis [79–80], have all been associated to the loss of CLN3 (or its ortholog Btn1p). A new phenotype, the cell motility defect described here, could indicate further cell migration phenotypes in other cell types during development, which will be the focus of future studies, and could reveal specific cell populations where the previously described phenotypes of $Cln3^{-/-}$ may be particularly important. Through interactions with several proteins [8, 12–14], CLN3 appears to have functions in the cell periphery, possibly through unique vesicular structures or lysosomes associated to specific cell regions, such as the neuronal synapse, or in recycling endocytosis. The present study contributes a novel interaction to an evolving interactome of CLN3 with nonmuscle myosin-IIB.

Myosin-IIB has been shown to play a role in the migration of granule cells in the developing cerebellum [81]. Normally, cerebellum granule cells undergo proliferation in the external granule cell layer, differentiate, and migrate radially to their final residence in the internal granule cell layer. Molecular motors play a crucial role in this process. It has been shown that when a point mutation is introduced into an evolutionarily conserved residue in the motor domain of myosin-IIB, the migration of a number of cell types including cerebellar granule cells is retarded in these mutant mice [64]. This thinning of the internal granule cell layer may precipitate the ataxia and cerebellar-specific motor abnormalities seen in these mice. Clinical studies indicate motor coordination defects in JNCL patients similar to phenotypes seen in transgenic mice by latency to fall from accelerating rotarod in both $Cln3^{-/-}$ mice [7], and also in $Myh10^{-/-}$ mice [65]. This common deficit in motor coordination could indicate that the cerebellum is a possible brain region where the myosin-IIB-CLN3 interaction may impact functional phenotypes in vivo, and future experiments examining this interaction in the cerebellum directly will be completed. Because myosin-IIB has been implicated in so many neuronal-specific functions, and is the exclusive non-muscle myosin-II expressed at certain stages of brain development, it is tempting to assign a significant consequence to these associations of myosin-IIB, CLN3, neurodevelopment and neurodegenerative disease. At this time, it would be premature to make conclusions; however, as we further our studies on this interaction, we will focus on identifying not only the specific physiological and functional requirements for this interaction, but also how the loss of this interaction contributes to the pathogenesis of JNCL.

Supplementary Material

Refer to Web version on PubMed Central for supplementary material.

Acknowledgments

Abbreviations

2D	two-dimension
ANOVA	analysis of variance
BrdU	5-bromo-2-deoxyuridine
CNS	central nervous system
DAPI	4′-6-Diamidino-2-phenylindole
DMEM	Dulbecco's Modified Eagle Medium
EDTA	ethylenediaminetetraacetic acid
FBS	fetal bovine serum
JNCL	Juvenile-neuronal ceroid lipofuscinosis
LAMP1	lysosomal associated membrane protein-1
MEF	mouse embryonic fibroblast
MTT	3-(4,5-Dimethylthiazol-2-yl)-2,5-diphenyltetrazolium bromide
Myh10	nonmuscle-myosin-IIB gene in mouse
Myh9	nonmuscle myosin-IIA gene in mouse
NCL	neuronal ceroid lipofuscinosis
pCMV	cytomegalovirus promoter
TBS	tris-buffered saline
Y2H	yeast-2-hybrid

References

1. Goebel HH. The neuronal ceroid-lipofuscinoses. J Child Neurol. 1995; 10:424–437. [PubMed: 8576551]

2. Consortium BD. Isolation of a novel gene underlying Batten disease, CLN3. The International Batten Disease Consortium. Cell. 1995; 82:949–957. [PubMed: 7553855]

3. Mole, SE. NCL Mutation Database. 2009. http://www.ucl.ac.uk/ncl/mutation.shtml

4. Pontikis CC, Cotman SL, MacDonald ME, Cooper JD. Thalamocortical neuron loss and localized astrocytosis in the Cln3Deltaex7/8 knock-in mouse model of Batten disease. Neurobiol Dis. 2005; 20:823–836. [PubMed: 16006136]

5. Pontikis CC, Cella CV, Parihar N, Lim MJ, Chakrabarti S, Mitchison HM, Mobley WC, Rezaie P, Pearce DA, Cooper JD. Late onset neurodegeneration in the Cln3−/− mouse model of juvenile neuronal ceroid lipofuscinosis is preceded by low level glial activation. Brain Res. 2004; 1023:231–242. [PubMed: 15374749]

6. Weimer JM, Custer AW, Benedict JW, Alexander NA, Kingsley E, Federoff HJ, Cooper JD, Pearce DA. Visual deficits in a mouse model of Batten disease are the result of optic nerve degeneration

and loss of dorsal lateral geniculate thalamic neurons. Neurobiol Dis. 2006; 22:284–293. [PubMed: 16412658]

7. Weimer JM, Benedict JW, Getty AL, Pontikis CC, Lim MJ, Cooper JD, Pearce DA. Cerebellar defects in a mouse model of juvenile neuronal ceroid lipofuscinosis. Brain Res. 2009; 1266:93–107. [PubMed: 19230832]

8. Luiro K, Yliannala K, Ahtiainen L, Maunu H, Jarvela I, Kyttala A, Jalanko A. Interconnections of CLN3, Hook1 and Rab proteins link Batten disease to defects in the endocytic pathway. Hum Mol Genet. 2004; 13:3017–3027. [PubMed: 15471887]

9. Ramirez-Montealegre D, Pearce DA. Defective lysosomal arginine transport in juvenile Batten disease. Hum Mol Genet. 2005; 14:3759–3773. [PubMed: 16251196]

10. Kyttala A, Yliannala K, Schu P, Jalanko A, Luzio JP. AP-1 and AP-3 facilitate lysosomal targeting of Batten disease protein CLN3 via its dileucine motif. J Biol Chem. 2005; 280:10277–10283. [PubMed: 15598649]

11. Phillips SN, Benedict JW, Weimer JM, Pearce DA. CLN3, the protein associated with batten disease: structure, function and localization. J Neurosci Res. 2005; 79:573–583. [PubMed: 15657902]

12. Chang JW, Choi H, Kim HJ, Jo DG, Jeon YJ, Noh JY, Park WJ, Jung YK. Neuronal vulnerability of CLN3 deletion to calcium-induced cytotoxicity is mediated by calsenilin. Hum Mol Genet. 2007; 16:317–326. [PubMed: 17189291]

13. Uusi-Rauva K, Luiro K, Tanhuanpaa K, Kopra O, Martin-Vasallo P, Kyttala A, Jalanko A. Novel interactions of CLN3 protein link Batten disease to dysregulation of fodrin-Na+, K+ ATPase complex. Exp Cell Res. 2008; 314:2895–2905. [PubMed: 18621045]

14. Vitiello SP, Benedict JW, Padilla-Lopez S, Pearce DA. Interaction between Sdo1p and Btn1p in the Saccharomyces cerevisiae model for Batten disease. Hum Mol Genet. 2010; 19:931–942. [PubMed: 20015955]

15. Takeda K, Kishi H, Ma X, Yu ZX, Adelstein RS. Ablation and mutation of nonmuscle myosin heavy chain II-B results in a defect in cardiac myocyte cytokinesis. Circ Res. 2003; 93:330–337. [PubMed: 12893741]

16. Lo CM, Buxton DB, Chua GC, Dembo M, Adelstein RS, Wang YL. Nonmuscle myosin IIb is involved in the guidance of fibroblast migration. Mol Biol Cell. 2004; 15:982–989. [PubMed: 14699073]

17. Vicente-Manzanares M, Koach MA, Whitmore L, Lamers ML, Horwitz AF. Segregation and activation of myosin IIB creates a rear in migrating cells. J Cell Biol. 2008; 183:543–554. [PubMed: 18955554]

18. Vicente-Manzanares M, Zareno J, Whitmore L, Choi CK, Horwitz AF. Regulation of protrusion, adhesion dynamics, and polarity by myosins IIA and IIB in migrating cells. J Cell Biol. 2007; 176:573–580. [PubMed: 17312025]

19. Wylie SR, Chantler PD. Separate but linked functions of conventional myosins modulate adhesion and neurite outgrowth. Nat Cell Biol. 2001; 3:88–92. [PubMed: 11146631]

20. Heath KE, Campos-Barros A, Toren A, Rozenfeld-Granot G, Carlsson LE, Savige J, Denison JC, Gregory MC, White JG, Barker DF, Greinacher A, Epstein CJ, Glucksman MJ, Martignetti JA. Nonmuscle myosin heavy chain IIA mutations define a spectrum of autosomal dominant macrothrombocytopenias: May-Hegglin anomaly and Fechtner, Sebastian, Epstein, and Alport-like syndromes. Am J Hum Genet. 2001; 69:1033–1045. [PubMed: 11590545]

21. Marqueze-Pouey B, Martin-Moutot N, Sakkou-Norton M, Leveque C, Ji Y, Cornet V, Hsiao WL, Seagar M. Toxicity and endocytosis of spinocerebellar ataxia type 6 polyglutamine domains: role of myosin IIb. Traffic. 2008; 9:1088–1100. [PubMed: 18384641]

22. Ryu J, Liu L, Wong TP, Wu DC, Burette A, Weinberg R, Wang YT, Sheng M. A critical role for myosin IIb in dendritic spine morphology and synaptic function. Neuron. 2006; 49:175–182. [PubMed: 16423692]

23. Bridgman PC, Dave S, Asnes CF, Tullio AN, Adelstein RS. Myosin IIB is required for growth cone motility. J Neurosci. 2001; 21:6159–6169. [PubMed: 11487639]

24. Takagishi Y, Futaki S, Itoh K, Espreafico EM, Murakami N, Murata Y, Mochida S. Localization of myosin II and V isoforms in cultured rat sympathetic neurones and their potential involvement in presynaptic function. J Physiol. 2005; 569:195–208. [PubMed: 16166155]

25. Conti MA, Adelstein RS. Nonmuscle myosin II moves in new directions. J Cell Sci. 2008; 121:11–18. [PubMed: 18096687]

26. Seehafer SS, Pearce DA. Spectral properties and mechanisms that underlie autofluorescent accumulations in Batten disease. Biochem Biophys Res Commun. 2009; 382:247–251. [PubMed: 19248764]

27. Rosenberger G, Gal A, Kutsche K. AlphaPIX associates with calpain 4, the small subunit of calpain, and has a dual role in integrin-mediated cell spreading. J Biol Chem. 2005; 280:6879–6889. [PubMed: 15611136]

28. Cottone CD, Chattopadhyay S, Pearce DA. Searching for interacting partners of CLN1, CLN2 and Btn1p with the two-hybrid system. Eur J Paediatr Neurol. 2001; 5(Suppl A):95–98. [PubMed: 11589016]

29. Weimer JM, Chattopadhyay S, Custer AW, Pearce DA. Elevation of Hook1 in a disease model of Batten disease does not affect a novel interaction between Ankyrin G and Hook1. Biochem Biophys Res Commun. 2005; 330:1176–1181. [PubMed: 15823567]

30. Mitchison HM, Bernard DJ, Greene ND, Cooper JD, Junaid MA, Pullarkat RK, de Vos N, Breuning MH, Owens JW, Mobley WC, Gardiner RM, Lake BD, Taschner PE, Nussbaum RL. Targeted disruption of the Cln3 gene provides a mouse model for Batten disease. The Batten Mouse Model Consortium [corrected]. Neurobiol Dis. 1999; 6:321–334. [PubMed: 10527801]

31. Chan CH, Mitchison HM, Pearce DA. Transcript and in silico analysis of CLN3 in juvenile neuronal ceroid lipofuscinosis and associated mouse models. Hum Mol Genet. 2008; 17:3332–3339. [PubMed: 18678598]

32. Elshatory Y, Brooks AI, Chattopadhyay S, Curran TM, Gupta P, Ramalingam V, Hofmann SL, Pearce DA. Early changes in gene expression in two models of Batten disease. FEBS Lett. 2003; 538:207–212. [PubMed: 12633880]

33. Weimer JM, Benedict JW, Elshatory YM, Short DW, Ramirez-Montealegre D, Ryan DA, Alexander NA, Federoff HJ, Cooper JD, Pearce DA. Alterations in striatal dopamine catabolism precede loss of substantia nigra neurons in a mouse model of juvenile neuronal ceroid lipofuscinosis. Brain Res. 2007; 1162:98–112. [PubMed: 17617387]

34. Kovacs AD, Weimer JM, Pearce DA. Selectively increased sensitivity of cerebellar granule cells to AMPA receptor-mediated excitotoxicity in a mouse model of Batten disease. Neurobiol Dis. 2006; 22:575–585. [PubMed: 16483786]

35. Quilliam LA, Huff SY, Rabun KM, Wei W, Park W, Broek D, Der CJ. Membrane-targeting potentiates guanine nucleotide exchange factor CDC25 and SOS1 activation of Ras transforming activity. Proc Natl Acad Sci U S A. 1994; 91:8512–8516. [PubMed: 8078913]

36. Ezaki J, Takeda-Ezaki M, Koike M, Ohsawa Y, Taka H, Mineki R, Murayama K, Uchiyama Y, Ueno T, Kominami E. Characterization of Cln3p, the gene product responsible for juvenile neuronal ceroid lipofuscinosis, as a lysosomal integral membrane glycoprotein. J Neurochem. 2003; 87:1296–1308. [PubMed: 14622109]

37. Kyttala A, Ihrke G, Vesa J, Schell MJ, Luzio JP. Two motifs target Batten disease protein CLN3 to lysosomes in transfected nonneuronal and neuronal cells. Mol Biol Cell. 2004; 15:1313–1323. [PubMed: 14699076]

38. Swailes NT, Colegrave M, Knight PJ, Peckham M. Non-muscle myosins 2A and 2B drive changes in cell morphology that occur as myoblasts align and fuse. J Cell Sci. 2006; 119:3561–3570. [PubMed: 16895968]

39. Vicente-Manzanares M, Ma X, Adelstein RS, Horwitz AR. Non-muscle myosin II takes centre stage in cell adhesion and migration. Nat Rev Mol Cell Biol. 2009; 10:778–790. [PubMed: 19851336]

40. Beadle C, Assanah MC, Monzo P, Vallee R, Rosenfeld SS, Canoll P. The role of myosin II in glioma invasion of the brain. Mol Biol Cell. 2008; 19:3357–3368. [PubMed: 18495866]

41. Bindschadler M, McGrath JL. Sheet migration by wounded monolayers as an emergent property of single-cell dynamics. J Cell Sci. 2007; 120:876–884. [PubMed: 17298977]

42. Gage FH. Mammalian neural stem cells. Science. 2000; 287:1433–1438. [PubMed: 10688783]

43. Allingham JS, Smith R, Rayment I. The structural basis of blebbistatin inhibition and specificity for myosin II. Nat Struct Mol Biol. 2005; 12:378–379. [PubMed: 15750603]

44. Song JW, Misgeld T, Kang H, Knecht S, Lu J, Cao Y, Cotman SL, Bishop DL, Lichtman JW. Lysosomal activity associated with developmental axon pruning. J Neurosci. 2008; 28:8993–9001. [PubMed: 18768693]

45. Metcalf DJ, Calvi AA, Seaman M, Mitchison HM, Cutler DF. Loss of the Batten disease gene CLN3 prevents exit from the TGN of the mannose 6-phosphate receptor. Traffic. 2008; 9:1905–1914. [PubMed: 18817525]

46. Pohl S, Mitchison HM, Kohlschutter A, van Diggelen O, Braulke T, Storch S. Increased expression of lysosomal acid phosphatase in CLN3-defective cells and mouse brain tissue. J Neurochem. 2007; 103:2177–2188. [PubMed: 17868323]

47. Michihara A, Toda K, Kubo T, Fujiwara Y, Akasaki K, Tsuji H. Disruptive effect of chloroquine on lysosomes in cultured rat hepatocytes. Biol Pharm Bull. 2005; 28:947–951. [PubMed: 15930724]

48. Gonzalez-Noriega A, Grubb JH, Talkad V, Sly WS. Chloroquine inhibits lysosomal enzyme pinocytosis and enhances lysosomal enzyme secretion by impairing receptor recycling. J Cell Biol. 1980; 85:839–852. [PubMed: 7190150]

49. Pearce DA, Nosel SA, Sherman F. Studies of pH regulation by Btn1p, the yeast homolog of human Cln3p. Mol Genet Metab. 1999; 66:320–323. [PubMed: 10191121]

50. Golabek AA, Kida E, Walus M, Kaczmarski W, Michalewski M, Wisniewski KE. CLN3 protein regulates lysosomal pH and alters intracellular processing of Alzheimer's amyloid-beta protein precursor and cathepsin D in human cells. Mol Genet Metab. 2000; 70:203–213. [PubMed: 10924275]

51. Holopainen JM, Saarikoski J, Kinnunen PK, Jarvela I. Elevated lysosomal pH in neuronal ceroid lipofuscinoses (NCLs). Eur J Biochem. 2001; 268:5851–5856. [PubMed: 11722572]

52. Padilla-Lopez S, Pearce DA. Saccharomyces cerevisiae lacking Btn1p modulate vacuolar ATPase activity to regulate pH imbalance in the vacuole. J Biol Chem. 2006; 281:10273–10280. [PubMed: 16423829]

53. Codlin S, Haines RL, Burden JJ, Mole SE. Btn1 affects cytokinesis and cell-wall deposition by independent mechanisms, one of which is linked to dysregulation of vacuole pH. J Cell Sci. 2008; 121:2860–2870. [PubMed: 18697832]

54. Cao Y, Espinola JA, Fossale E, Massey AC, Cuervo AM, MacDonald ME, Cotman SL. Autophagy is disrupted in a knock-in mouse model of juvenile neuronal ceroid lipofuscinosis. J Biol Chem. 2006; 281:20483–20493. [PubMed: 16714284]

55. Bottger BA, Sjolund M, Thyberg J. Chloroquine and monensin inhibit induction of DNA synthesis in rat arterial smooth muscle cells stimulated with platelet-derived growth factor. Cell Tissue Res. 1988; 252:275–285. [PubMed: 3383211]

56. Codlin S, Haines RL, Mole SE. btn1 affects endocytosis, polarization of sterol-rich membrane domains and polarized growth in Schizosaccharomyces pombe. Traffic. 2008; 9:936–950. [PubMed: 18346214]

57. Togo T, Steinhardt RA. Nonmuscle myosin IIA and IIB have distinct functions in the exocytosis-dependent process of cell membrane repair. Mol Biol Cell. 2004; 15:688–695. [PubMed: 14617807]

58. Kolega J. Asymmetric distribution of myosin IIB in migrating endothelial cells is regulated by a rho-dependent kinase and contributes to tail retraction. Mol Biol Cell. 2003; 14:4745–4757. [PubMed: 12960430]

59. Zhang M, Rao PV. Blebbistatin, a novel inhibitor of myosin II ATPase activity, increases aqueous humor outflow facility in perfused enucleated porcine eyes. Invest Ophthalmol Vis Sci. 2005; 46:4130–4138. [PubMed: 16249490]

60. Tullio AN, Accili D, Ferrans VJ, Yu ZX, Takeda K, Grinberg A, Westphal H, Preston YA, Adelstein RS. Nonmuscle myosin II-B is required for normal development of the mouse heart. Proc Natl Acad Sci U S A. 1997; 94:12407–12412. [PubMed: 9356462]

61. Ma X, Bao J, Adelstein RS. Loss of cell adhesion causes hydrocephalus in nonmuscle myosin II-B-ablated and mutated mice. Mol Biol Cell. 2007; 18:2305–2312. [PubMed: 17429076]

62. Miyazaki T, Watanabe M, Yamagishi A, Takahashi M. B2 exon splicing of nonmuscle myosin heavy chain IIB is differently regulated in developing and adult rat brain. Neurosci Res. 2000; 37:299–306. [PubMed: 10958978]

63. Murakami N, Trenkner E, Elzinga M. Changes in expression of nonmuscle myosin heavy chain isoforms during muscle and nonmuscle tissue development. Dev Biol. 1993; 157:19–27. [PubMed: 8482409]

64. Ma X, Kawamoto S, Hara Y, Adelstein RS. A point mutation in the motor domain of nonmuscle myosin II-B impairs migration of distinct groups of neurons. Mol Biol Cell. 2004; 15:2568–2579. [PubMed: 15034141]

65. Ma X, Kawamoto S, Uribe J, Adelstein RS. Function of the neuron-specific alternatively spliced isoforms of nonmuscle myosin II-B during mouse brain development. Mol Biol Cell. 2006; 17:2138–2149. [PubMed: 16481398]

66. Belly A, Bodon G, Blot B, Bouron A, Sadoul R, Goldberg Y. CHMP2B mutants linked to frontotemporal dementia impair maturation of dendritic spines. J Cell Sci. 2010

67. Ishmael JE, Safic M, Amparan D, Vogel WK, Pham T, Marley K, Filtz TM, Maier CS. Nonmuscle myosins II-B and Va are components of detergent-resistant membrane skeletons derived from mouse forebrain. Brain Res. 2007; 1143:46–59. [PubMed: 17321505]

68. Rakheja D, Narayan SB, Pastor JV, Bennett MJ. CLN3P, the Batten disease protein, localizes to membrane lipid rafts (detergent-resistant membranes). Biochem Biophys Res Commun. 2004; 317:988–991. [PubMed: 15094366]

69. Hering H, Lin CC, Sheng M. Lipid rafts in the maintenance of synapses, dendritic spines, and surface AMPA receptor stability. J Neurosci. 2003; 23:3262–3271. [PubMed: 12716933]

70. Prasad VV, Pullarkat RK. Brain lysosomal hydrolases in neuronal ceroid-lipofuscinoses. Mol Chem Neuropathol. 1996; 29:169–179. [PubMed: 8971694]

71. Sleat DE, Sohar I, Pullarkat PS, Lobel P, Pullarkat RK. Specific alterations in levels of mannose 6-phosphorylated glycoproteins in different neuronal ceroid lipofuscinoses. Biochem J. 1998; 334(Pt 3):547–551. [PubMed: 9729460]

72. Stein CS, Yancey PH, Martins I, Sigmund RD, Stokes JB, Davidson BL. Osmoregulation of Ceroid Neuronal Lipofuscinosis Type 3 (CLN3) in the Renal Medulla. Am J Physiol Cell Physiol. 2010

73. Hobert JA, Dawson G. A novel role of the Batten disease gene CLN3: association with BMP synthesis. Biochem Biophys Res Commun. 2007; 358:111–116. [PubMed: 17482562]

74. Rusyn E, Mousallem T, Persaud-Sawin DA, Miller S, Boustany RM. CLN3p impacts galactosylceramide transport, raft morphology, and lipid content. Pediatr Res. 2008; 63:625–631. [PubMed: 18317235]

75. Ramirez-Montealegre D, Chattopadhyay S, Curran TM, Wasserfall C, Pritchard L, Schatz D, Petitto J, Hopkins D, She JX, Rothberg PG, Atkinson M, Pearce DA. Autoimmunity to glutamic acid decarboxylase in the neurodegenerative disorder Batten disease. Neurology. 2005; 64:743–745. [PubMed: 15728308]

76. Chan CH, Ramirez-Montealegre D, Pearce DA. Altered arginine metabolism in the central nervous system (CNS) of the Cln3−/− mouse model of juvenile Batten disease. Neuropathol Appl Neurobiol. 2009; 35:189–207. [PubMed: 19284480]

77. Pearce DA, Ferea T, Nosel SA, Das B, Sherman F. Action of BTN1, the yeast orthologue of the gene mutated in Batten disease. Nat Genet. 1999; 22:55–58. [PubMed: 10319861]

78. Pearce DA, Carr CJ, Das B, Sherman F. Phenotypic reversal of the btn1 defects in yeast by chloroquine: a yeast model for Batten disease. Proc Natl Acad Sci U S A. 1999; 96:11341–11345. [PubMed: 10500178]

79. Persaud-Sawin DA, VanDongen A, Boustany RM. Motifs within the CLN3 protein: modulation of cell growth rates and apoptosis. Hum Mol Genet. 2002; 11:2129–2142. [PubMed: 12189165]

80. Puranam KL, Guo WX, Qian WH, Nikbakht K, Boustany RM. CLN3 defines a novel antiapoptotic pathway operative in neurodegeneration and mediated by ceramide. Mol Genet Metab. 1999; 66:294–308. [PubMed: 10191118]

81. Persaud-Sawin DA, McNamara JO 2nd, Rylova S, Vandongen A, Boustany RM. A galactosylceramide binding domain is involved in trafficking of CLN3 from Golgi to rafts via recycling endosomes. Pediatr Res. 2004; 56:449–463. [PubMed: 15240864]
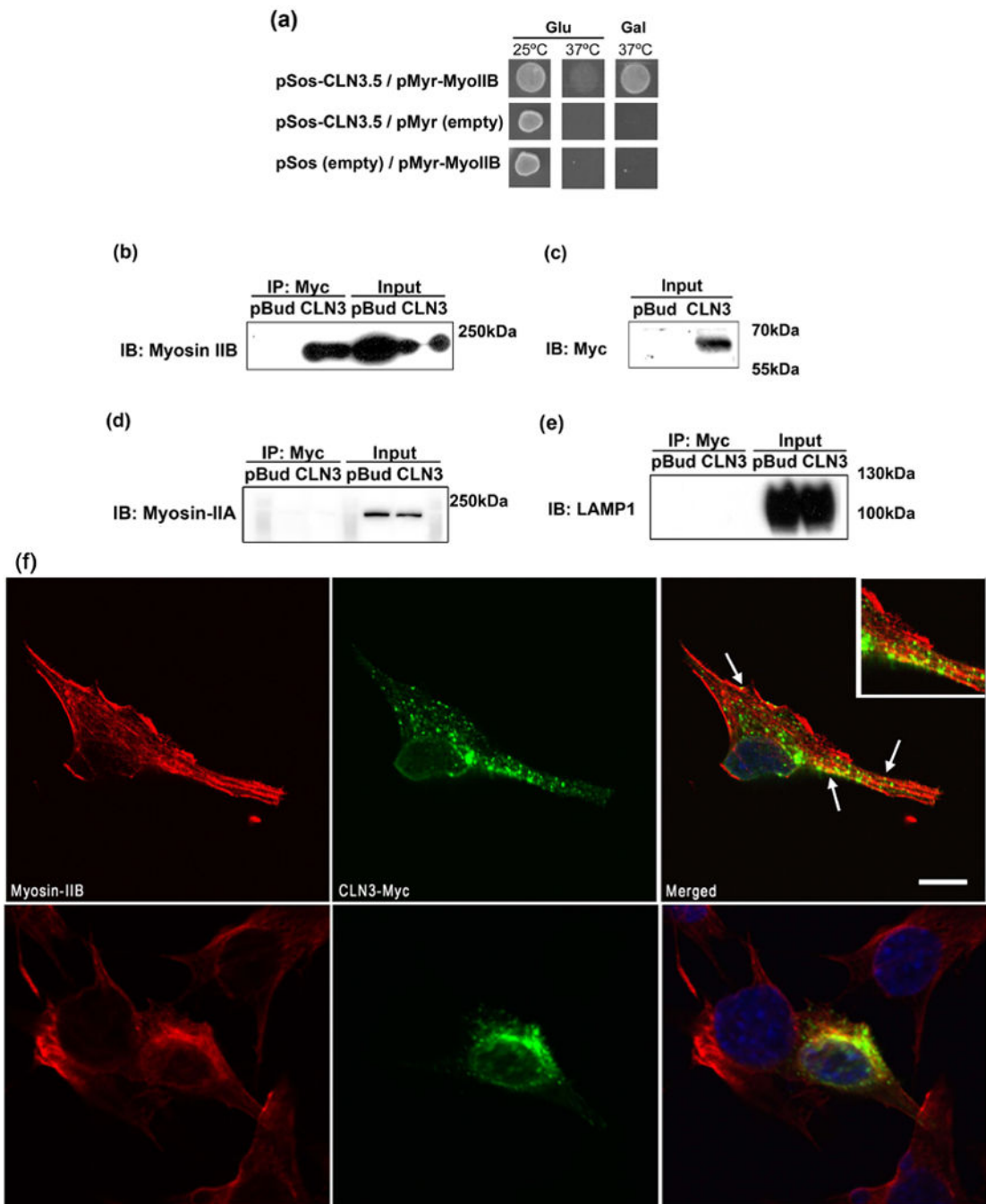
Figure 1. CLN3 interacts with myosin-IIB

The Cytotrap yeast two hybrid (Y2H) method was used to identify novel interacting partners of CLN3. pSos-CLN3.5 indicates the C-terminus CLN3 fusion with human Sos protein and pMyr-MyoIIB indicates a myristylated fragment of myosin-IIB that was identified in Y2H library screen. A positive interaction is identified when the transformed *cdc25H* yeast grow on galactoseat the permissive temperature of 37°C, which reveals suppression of the temperature sensitivity of this strain, only in the presence of both interacting proteins (a). We identified myosin-IIB as a protein that interacts with the C-terminus of CLN3.

Validation of this Y2H finding was performed using protein isolates from NIH/3T3 fibroblasts transfected with either empty vector (pBud) or myc-tagged CLN3 and immunoprecipitated with an anti-myc antibody. Immunoprecipitated proteins (b, lanes 1 and 2) and total lysates (b, lanes 3 and 4) were probed with anti-myosin-IIB antibody, confirming the interaction between CLN3 and endogenous myosin-IIB (b, lane 2). Myosin-IIB did not precipitate in the absence of CLN3 (b, lane 1). Lysates were probed with anti-myc antibody to confirm CLN3 expression (c). The interaction is specific to the myosin-IIB isoform, as myosin-IIA does not co-immunopreicipate with CLN3 (d). LAMP1, a lysosomal membrane protein that has not been shown to interact with CLN3, did not immunoprecipitate with CLN3 nonspecifically (e, lane 2). Merged images (yellow) reveal punctate specific co-localization of endogenous myosin-IIB (red) and transfected CLN3-myc (green) in NIH/3T3 fibroblasts (f). Images were acquired by confocal microscopy at 100×, scale is 25 μm.
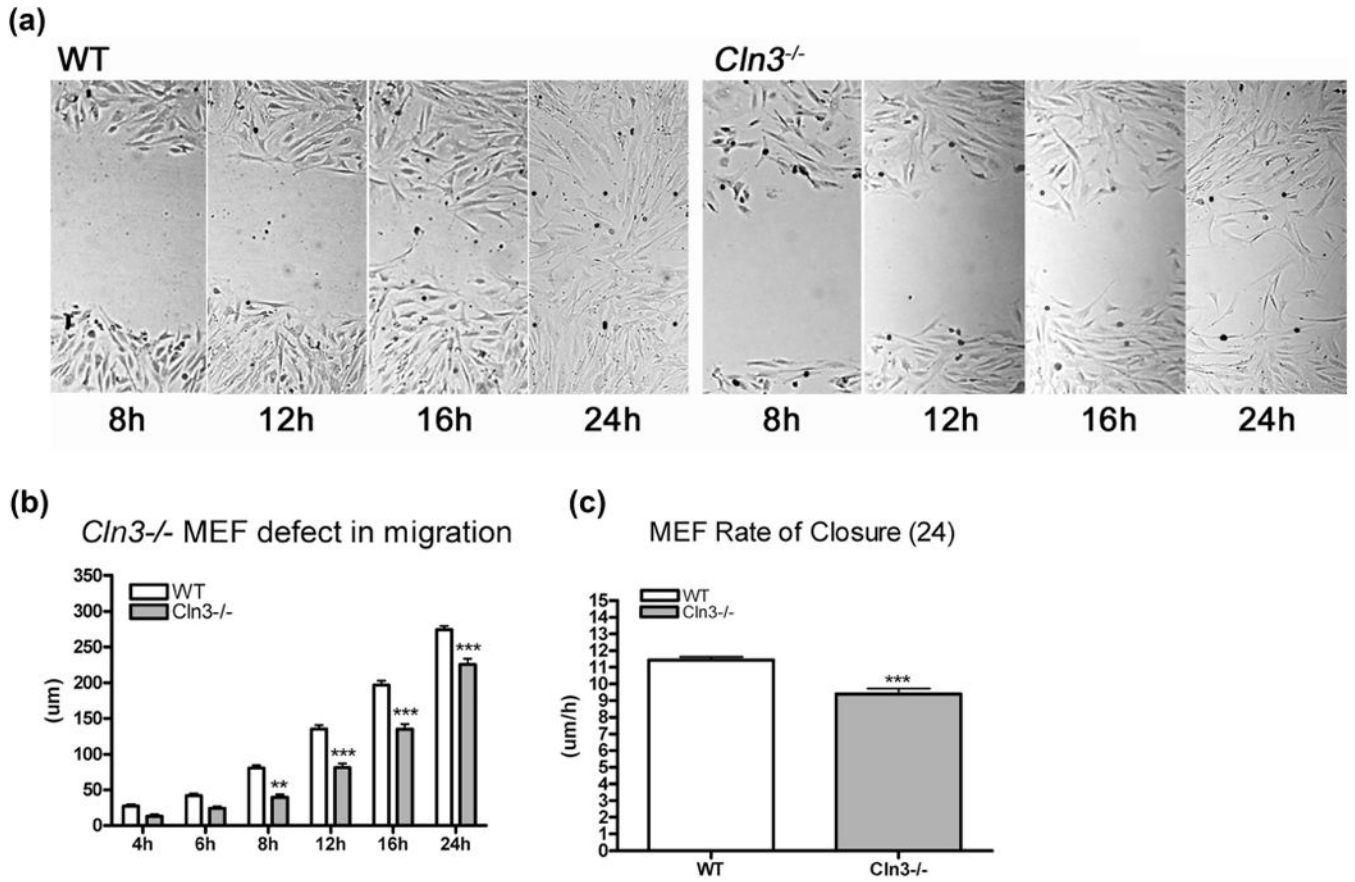
Figure 2. Fibroblast scratch assay reveals a migration defect in Cln3$^{-/-}$ cells
Cln3$^{-/-}$ MEF cells showed a delay in migration into the open substrate, beginning at 8 hours post-scratch (a). The distance each edge of cells traverses was calculated relative to the initial scratch distance (b). The rate of the scratch closure over 24 hours demonstrates that *Cln3$^{-/-}$* MEFs exhibit a defect in migration (c) (*** $p < 0.001$; **$p < 0.01$, 2-way ANOVA, Bonferroni Post-Hoc test). Data shown are mean ± SEM.
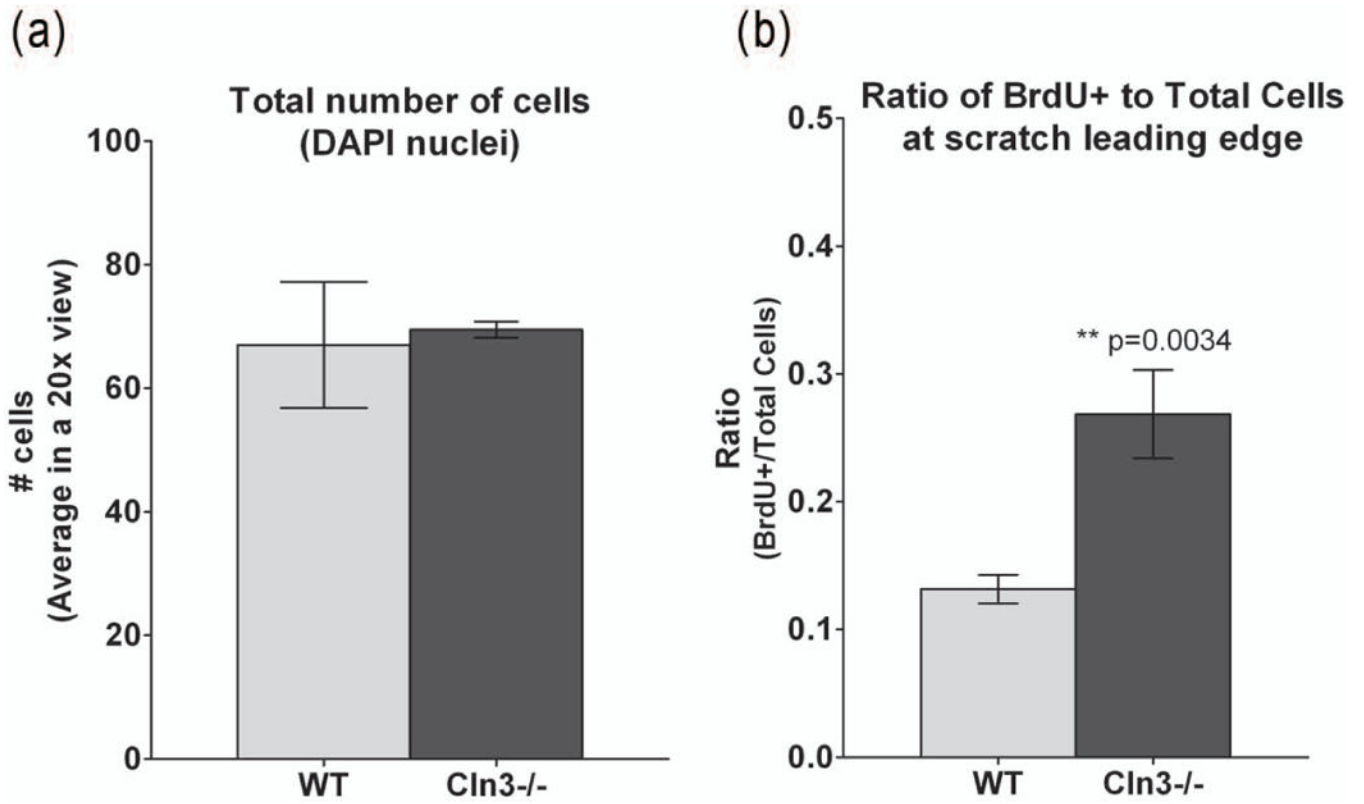
Figure 3. There are more actively proliferating Cln3$^{-/-}$ cells at the leading edge of the scratch
BrdU incorporation was observed following 8 hours MEF migration into the scratch. There was no difference in the total number of DAPI-stained nuclei at the leading edge of the scratch (a). However, the ratio of BrdU^{+} to total DAPI nuclei indicated a significant difference between *Cln3*$^{-/-}$ and WT cells (b). There are more BrdU^{+} *Cln3*$^{-/-}$ cells at the scratch leading edge. (** $p<0.001$, Student's t-test). Data shown are mean ± SEM.
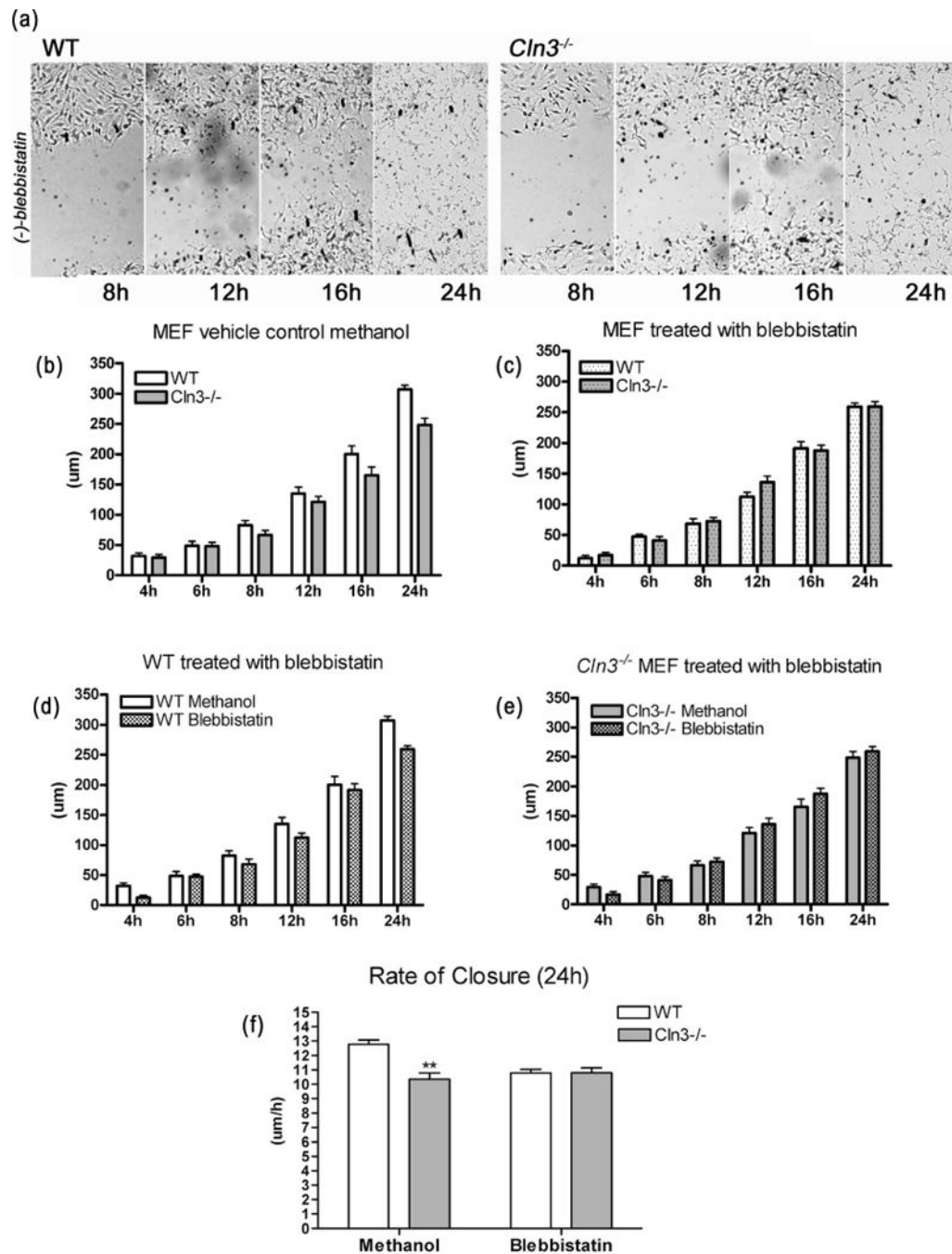
Figure 4. Inhibition of myosin-IIB with blebbistatin in wild type cells mimics the Cln3$^{-/-}$ phenotype

Following a scratch disruption to the confluent monolayer (0h), complete media was replaced with media containing 50 μm blebbistatin (a). Bright field representative images for WT (left panels) and *Cln3$^{-/-}$* (right panels) (a) demonstrate the change in morphology with blebbistatin treatment for both genotypes. The distance each leading edge of cells traverses into the scratched surface was calculated relative to the initial scratch distance in vehicle control (b) and 50 μm blebbistatin (c) treatment for WT (d) and *Cln3$^{-/-}$* (e) cells. *Cln3$^{-/-}$*

MEF cells showed a delay in migration into the open substrate, beginning at 8 hours post-scratch, which does not change with blebbistatin treatment (c). WT MEF migration rate is delayed by blebbistatin treatment over 24 hours (f). (2-way ANOVA; Bonferroni Post-Hoc test, *** p<0.001; **p<0.01). Data shown are mean ± SEM.
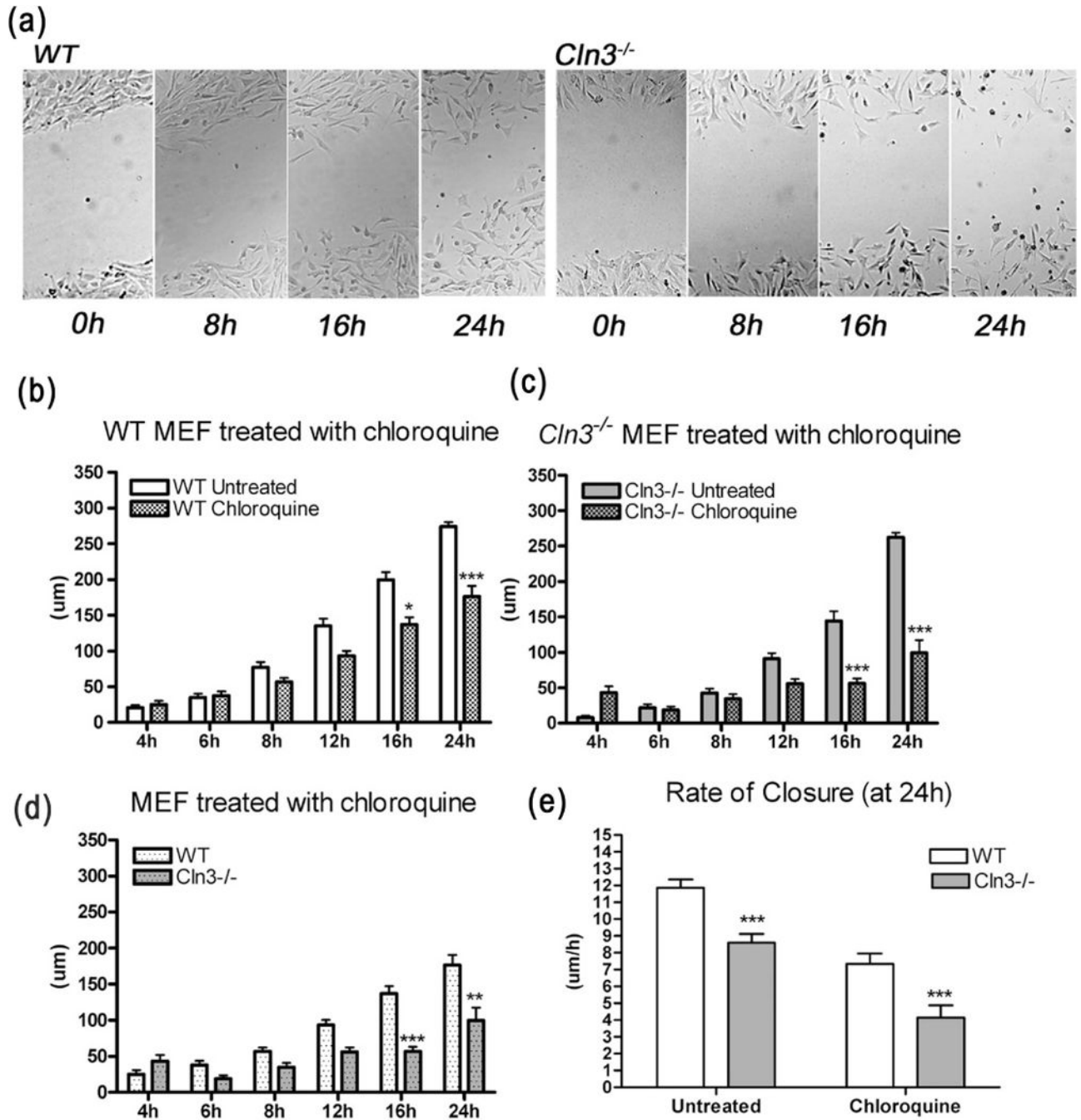
Figure 5. Treatment with chloroquine exacerbates the migration defect

During chloroquine treatment, WT cell migration is slowed (a,b). $Cln3^{-/-}$ MEF migration is further slowed by treatment with chloroquine (a,c). The WT MEF cells do close the scratch surface following a delay; however, $Cln3^{-/-}$ MEF cells are never able to overcome the effect of the chloroquine treatment and do not close the scratch, indicating that the difference between the genotypes is maintained (d). The rate of closure of both genotypes is reduced by chloroquine treatment (e). (*** $p<0.001$; **$p<0.01$, 2-way ANOVA; Bonferroni Post-Hoc test). Data shown are mean ± SEM.

Ratio of BrdU+ to Total Cells
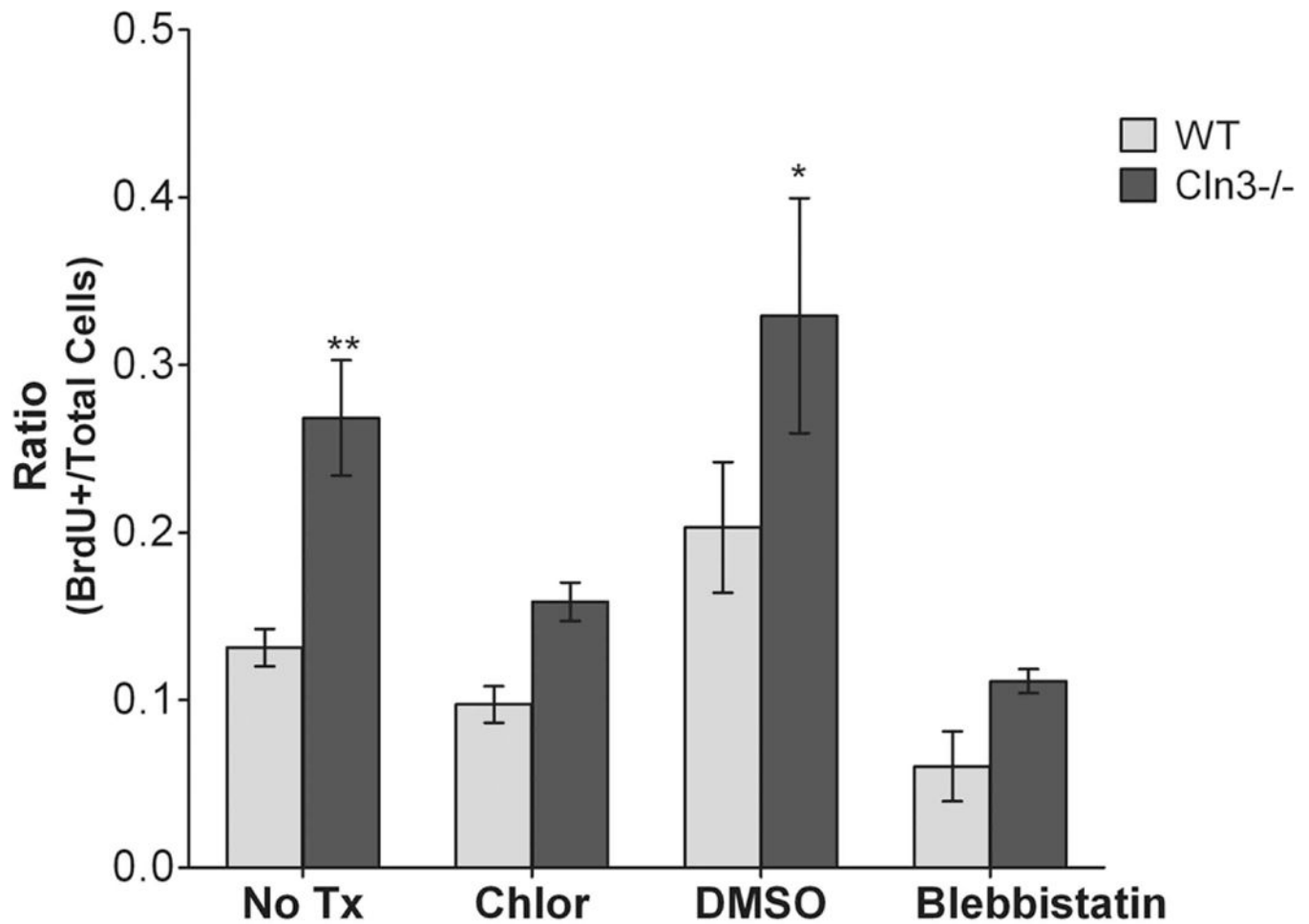
Figure 6. Chloroquine and blebbistatin treatment decrease the ratio of Cln3$^{-/-}$ BrdU^{+} cells
BrdU incorporation was observed following 8 hours MEF migration into the scratch under
treatment conditions used in the scratch assay. By 2-way ANOVA and Bonferroni Post-Hoc
tests, the ratio of BrdU+ to total DAPI nuclei is significantly greater without treatments (No
Tx) and in DMSO-vehicle controls, but not significantly different during chloroquine or
blebbistatin treatments (* $p<0.05$, ** $p<0.01$). Data shown are mean ± SEM.
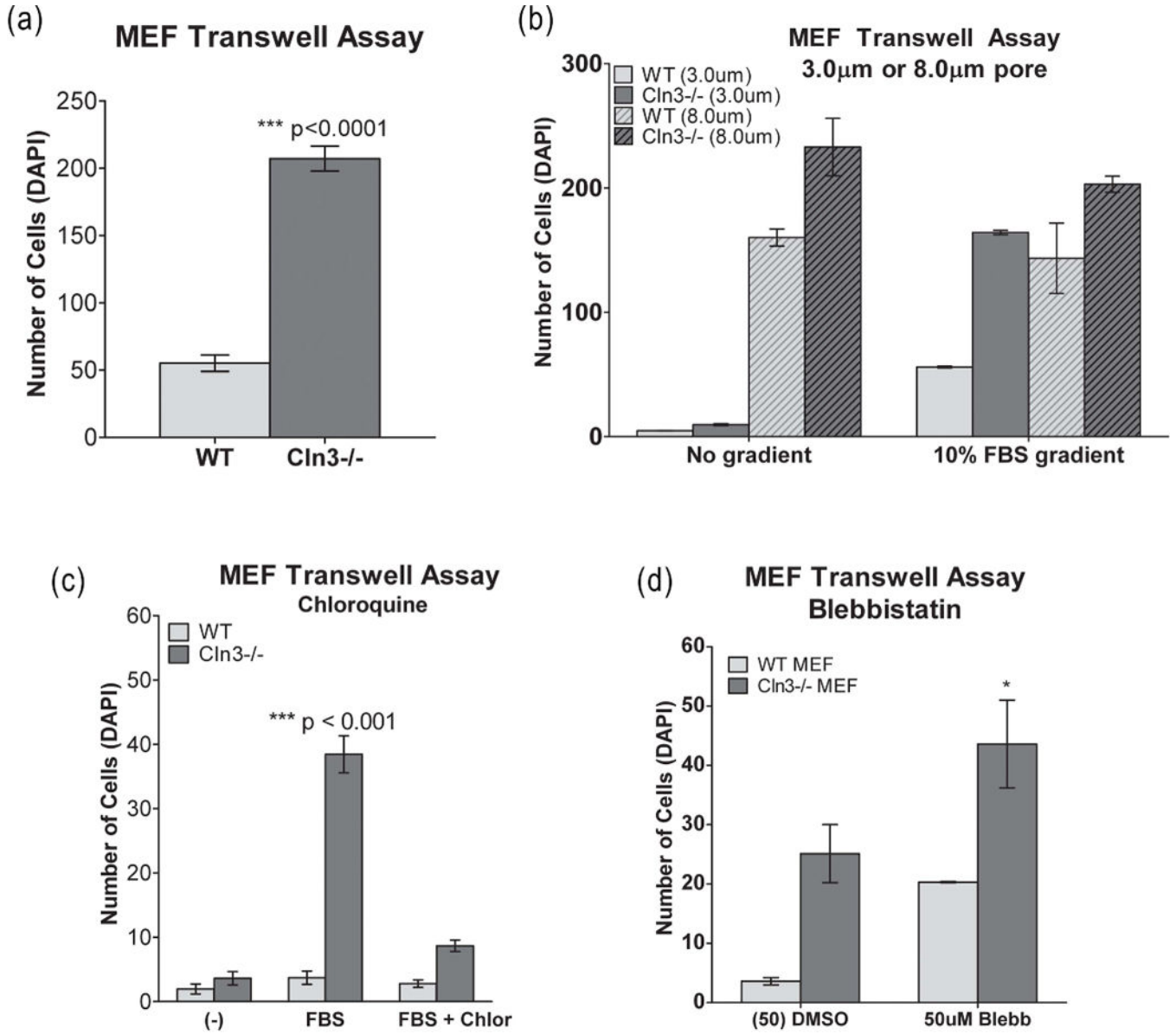
Figure 7. MEF chemotaxis through a gradient of trophic factors reveals a Cln3$^{-/-}$ phenotype
Cln3$^{-/-}$ cells migrate towards the source of rich media more than WT, indicating a particular sensitivity to these conditions (a) (p<0.001, Student's T-test). This phenotype requires a 3.0μm pore filter to provide selectivity, as an 8.0μm filter does not produce selection between the genotypes (b). Treatment with chloroquine prevents this movement of *Cln3$^{-/-}$* cells (c). Blebbistatin treatment causes an increase of WT and *Cln3$^{-/-}$* cells movement through the filter, however *Cln3$^{-/-}$* cells continue to move more readily through the filter (d). No gradient (serum-rich media in both chambers) was used as a negative control for all experiments. (*** p<0.001; **p<0.01, 2-way ANOVA; Bonferroni Post-Hoc test). Data shown are mean ± SEM.
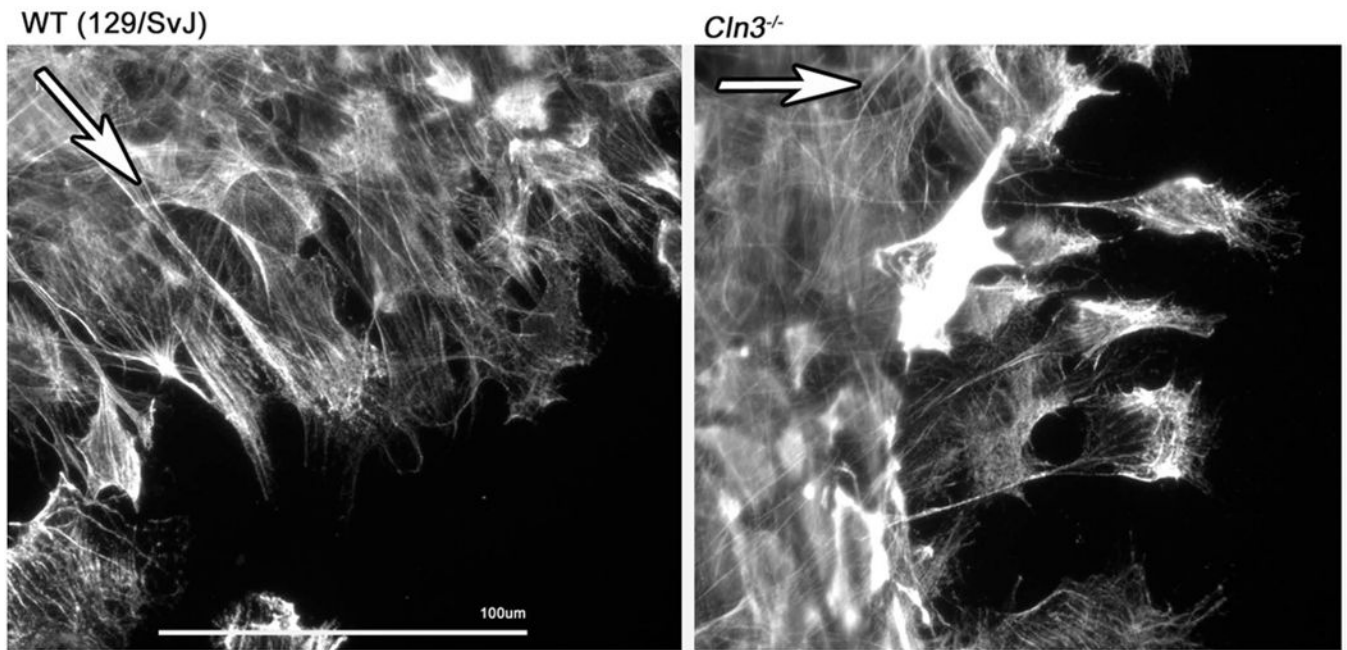
Figure 8. The morphology of Cln3$^{-/-}$ fibroblasts is elongated
MEF's after 8h of migration, stained with a monoclonal anti-myosin-IIB antibody. The arrow indicates the direction of cell migration. WT MEF cultures have a filamentous and even distribution of myosin-IIB as cells migrate (left panel). *Cln3$^{-/-}$* cells have a subtly different morphology, with an elongated tail and clusters of myosin-IIB at the leading edge of migrating cells (right panel). Scale is 100 μm, images were acquired at 40×.
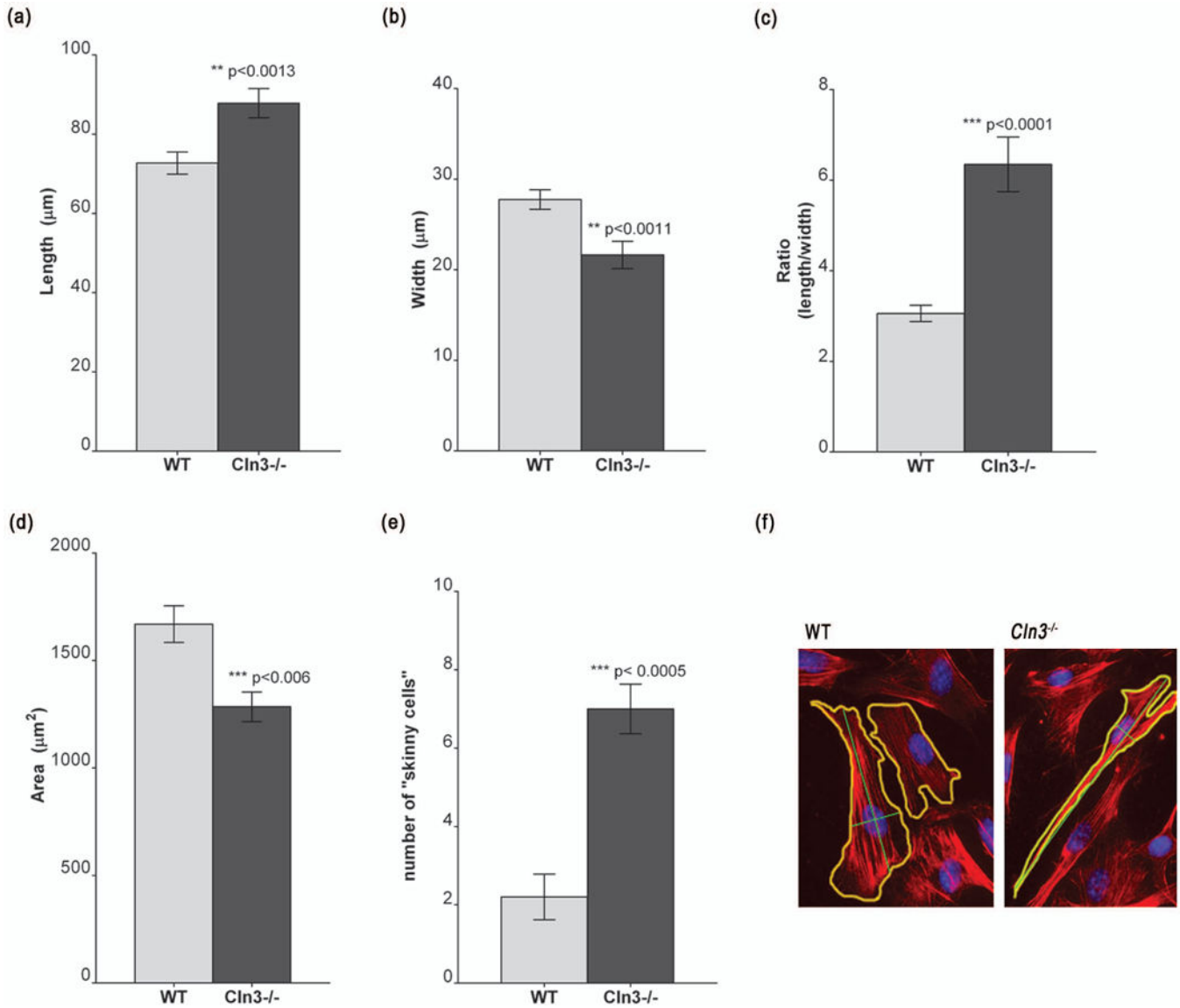
Figure 9. Cln3⁻/⁻ MEF's are longer and skinnier than WT

The elongated morphology of *Cln3⁻/⁻* MEFs can be quantified. Cells migrating into the scratch were stained with anti-myosin-IIB antibodies. *Cln3⁻/⁻* MEF cells are significantly longer in length (a) and shorter in width (b), and are significantly elongated by the ratio of length to width (c). *Cln3⁻/⁻* MEF cells have significantly smaller area of myosin-IIB staining than WT cells (d). Finally, the incidence of skinny cells per 20× field of view, is significantly higher for *Cln3⁻/⁻* MEFs (e). Representative images of WT and *Cln3⁻/⁻* MEF cells stained for myosin-IIB (red) and DAPI (blue) are shown with yellow lines indicating the area of myosin-IIB staining measured, and green lines indicating the length and width (f). At least 100 cells were examined for each genotype, from 5 randomly selected fields of view each at 20×. The representative image (f) scale is 50 μm. (**p<0.01, ***p<0.001, Student's T-test). Data shown are mean ± SEM.
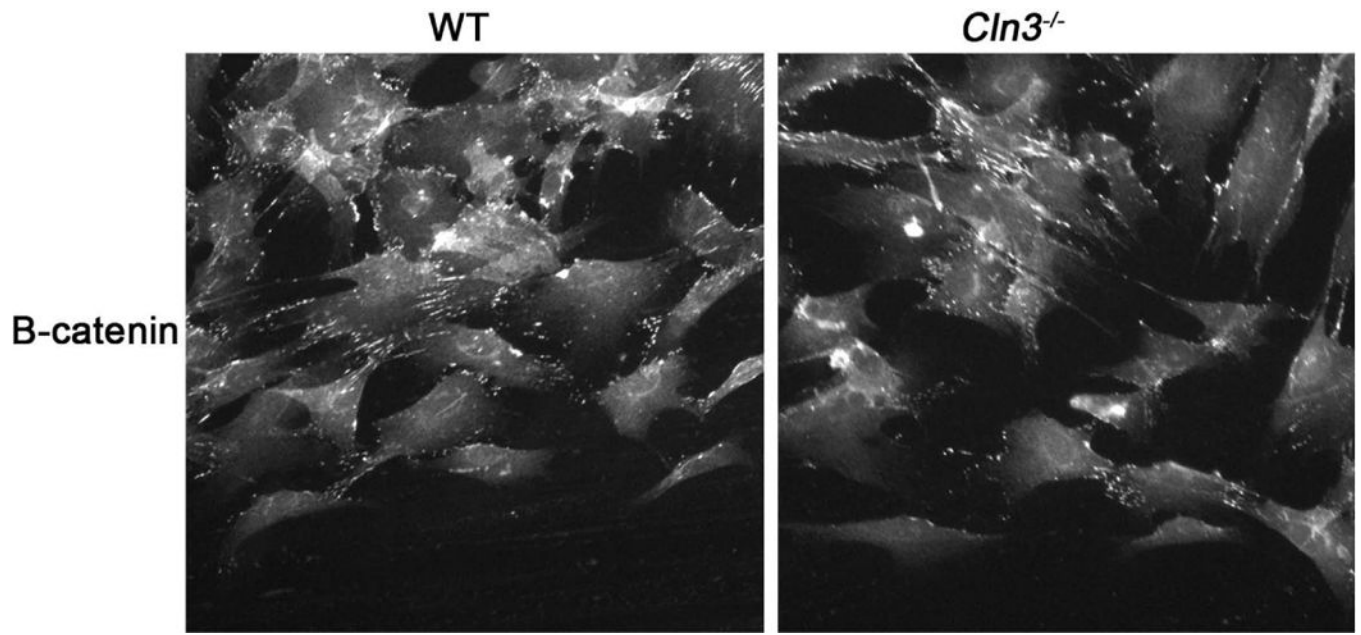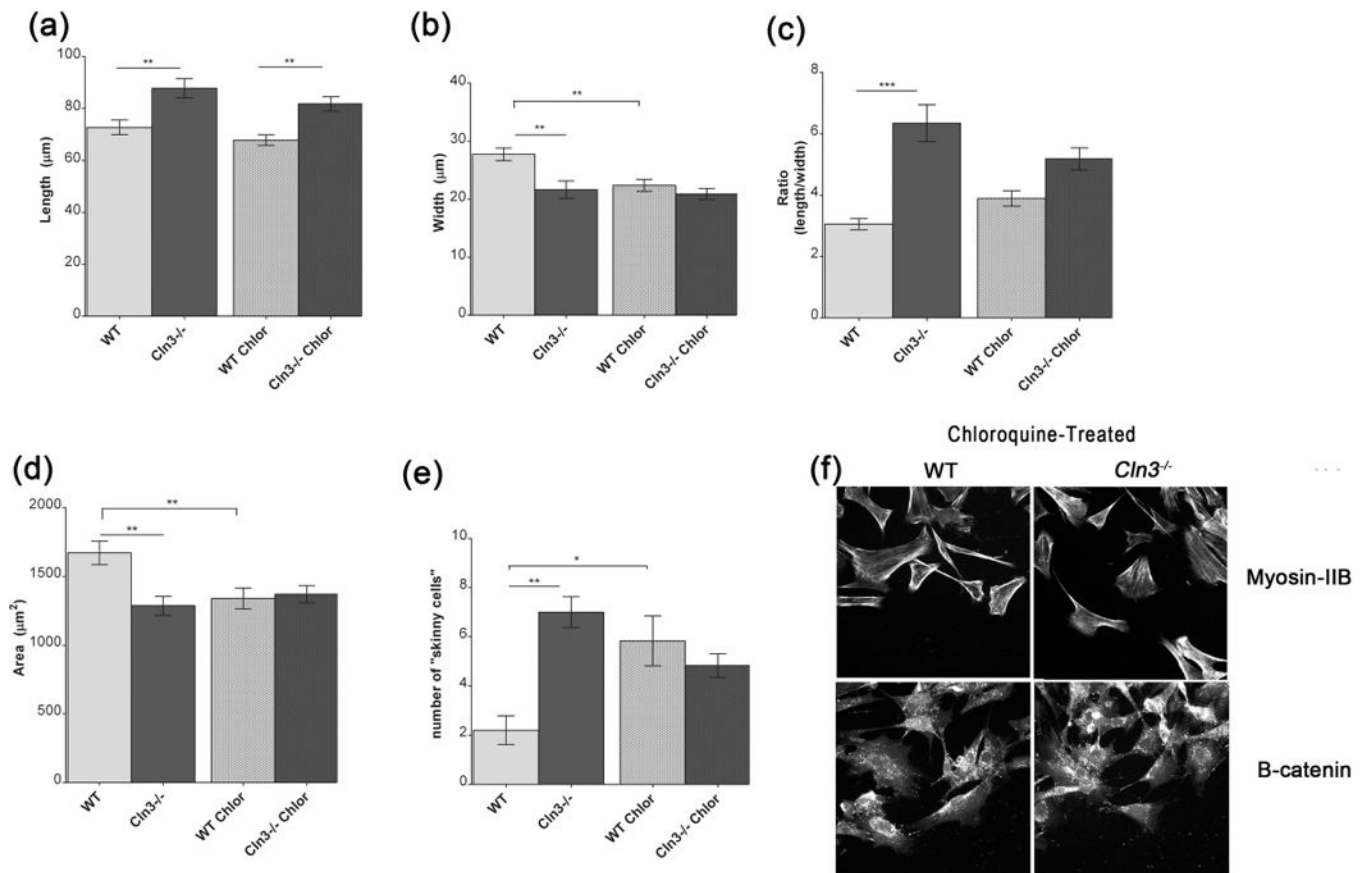
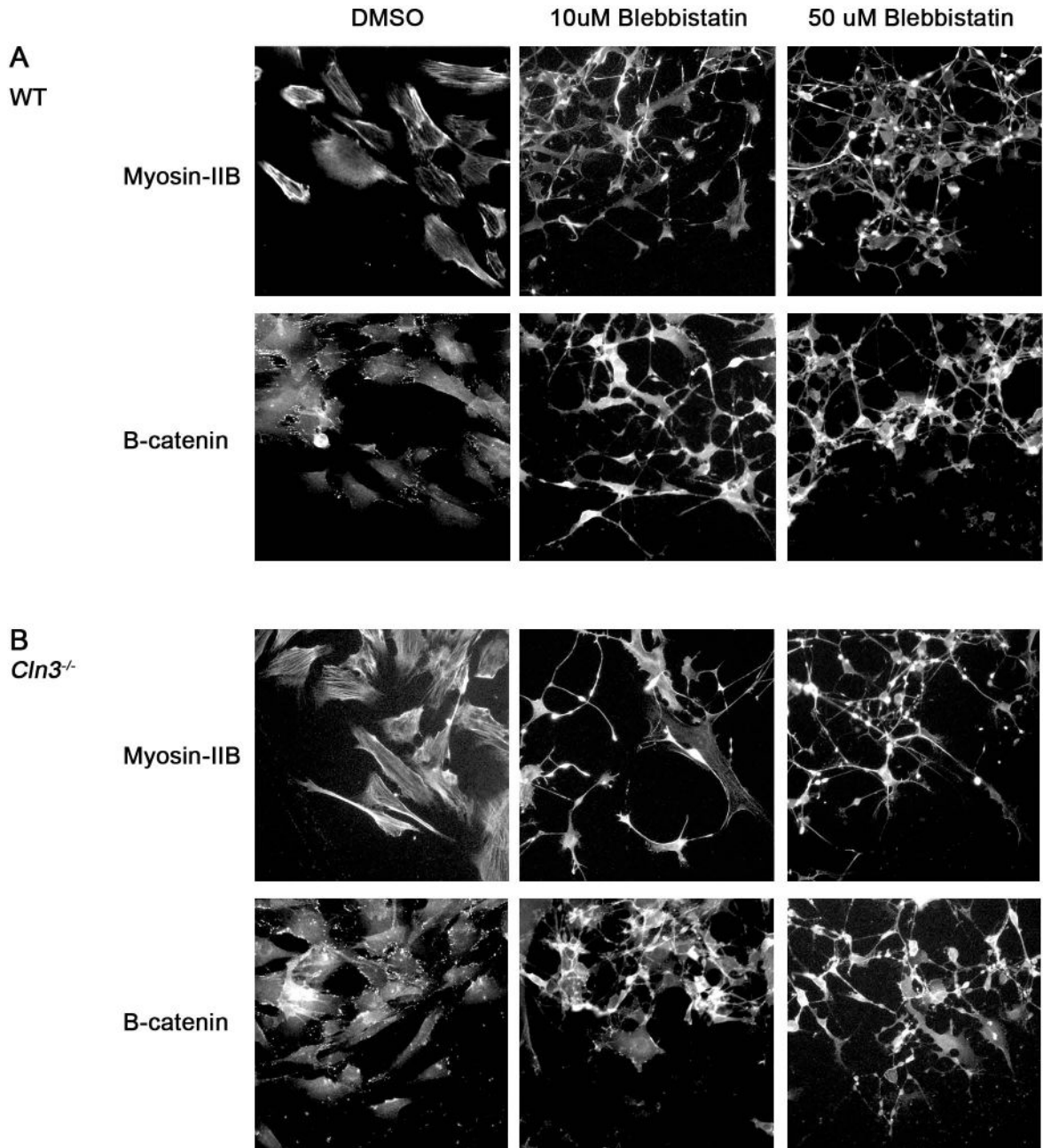**Figure 10. Adherens junction distribution in migrating MEF cells**
Adherens junctions in migrating *Cln3*−/− MEFs do not appear altered. WT (left panels) and *Cln3*−/− (right panels) MEF cells were stained with a monoclonal anti-β-catenin antibody as a marker for adherens junctions. Though there seems to be a subtle disorganization of β-catenin staining in *Cln3*−/− cells, there does not appear to be a gross difference in adherens junction distribution between genotypes. Images are 20×, the scale is 100 μm.

Figure 11. Myosin-IIB & adherens junctions distribution in migrating MEF cells treated with chloroquine

The length, width, and area of myosin-IIB distribution of cells migrating into the scratch during chloroquine treatment were measured. *Cln3*$^{-/-}$ MEF cells are significantly longer than WT during chloroquine treatment (abbreviated "Chlor") (a), but the width of WT MEF cells decreases with chloroquine treatment (b). The ratio of length to width is significantly greater in *Cln3*$^{-/-}$ without, but not with, chloroquine treatment (c). Chloroquine treatment reduces the area of WT cells (d). Finally, the number of WT skinny cells per 20× field of view significantly increases with chloroquine treatment for WT MEFs (e). Myosin-IIB distribution is collapsed slightly and adherens junction puncta (β-catenin staining) shift from the periphery of cells to perinuclear in both genotypes during chloroquine treatment (f). At least 120 cells were examined for each genotype, from 5 randomly selected fields of view each at 20×. Scale is 100 μm. (**$p < 0.01$, ***$p < 0.001$, 1-way ANOVA, Bonferroni Post-Hoc tests). Data shown are mean ± SEM.

Figure 12. Myosin-IIB & adherens junctions distribution in migrating MEF cells treated with blebbistatin

Blebbistatin treatment of migrating MEFs causes changes in the myosin-IIB associated cytoskeleton and cell morphology. There is no difference in adherens junction distribution between genotypes following treatment with blebbistatin. WT (a–f) and $Cln3^{-/-}$ (g–l) MEF cells were grown on coverslips, subjected to a scratch, and 8 hours after the scratch were fixed and stained for myosin-IIB (a–c; g–i) and β-catenin (d–f; j–l). Myosin-IIB staining indicates intact cytoskeleton in migrating MEFs in both genotypes without blebbistatin treatment (a and g). Blebbistatin treatment causes the cells to elongate and "bleb" as the myosin-IIB associated cytoskeleton collapses (b, c, h, i). While WT cells constrict even with

low (10μM) blebbistatin (b), *Cln3*^{−/−} cells exhibit some regions that are not completely collapsed with myosin-II inhibition (h). At higher concentrations of blebbistatin (50μM), *Cln3*^{−/−} cells are completely collapsed as WT (i). β-catenin staining indicates the placement of adherens junctions in WT (d–f) and *Cln3*^{−/−} (j–l). Both genotypes exhibit diffuse staining of β-catenin with blebbistatin treatment (e, f; k, l). Images are representative of morphology and staining typically observed in numerous cultures treated similarly. Scale is 100 μm.
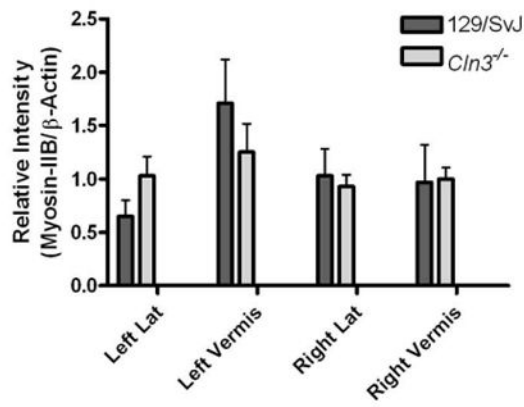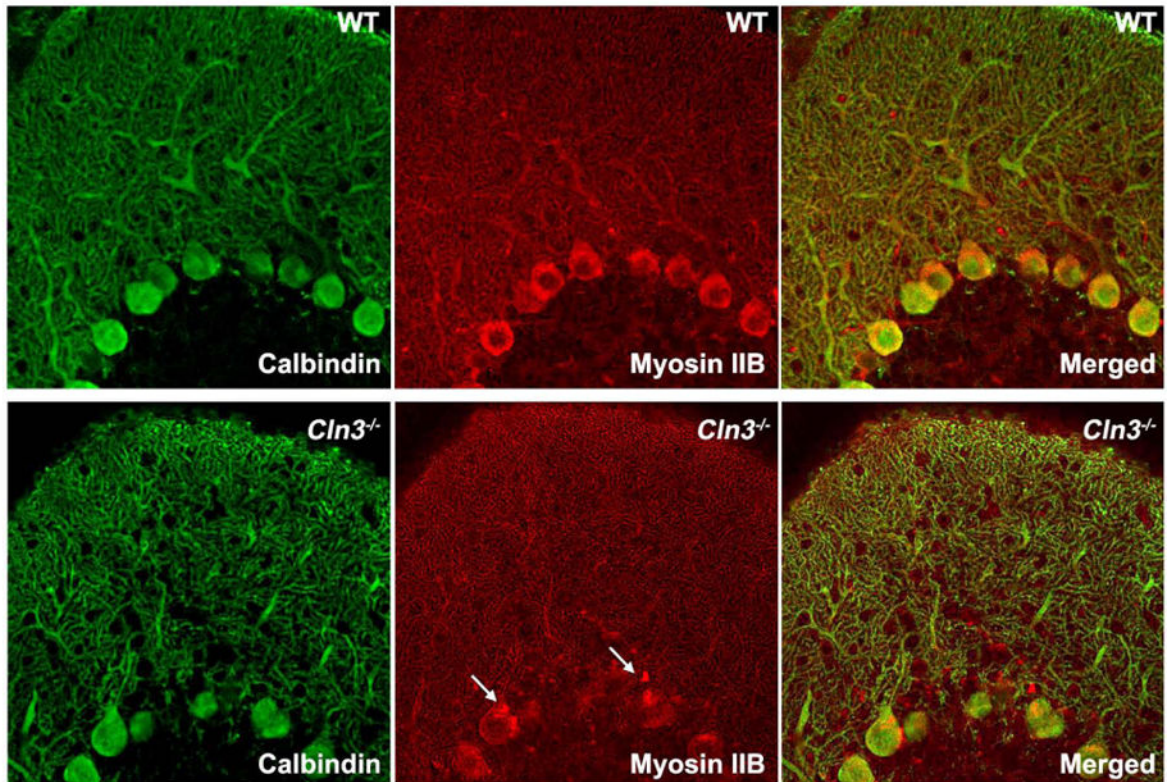
Figure 13. Myosin-IIB expression and differential localization in Cln3⁻/⁻ mouse cerebellum
Examination of the relative expression levels of myosin-IIB in the cerebellum by Western blotting, anatomically separated into four regions [left and right lateral hemispheres and vermis], revealed no obvious changes in the abundance of this protein in the *Cln3⁻/⁻* cerebellum (a). In some Purkinje cells (anti-calbindin, green) within the *Cln3⁻/⁻* cerebellum, there was an abnormal punctate myosin-IIB staining (red) not observed in WT Purkinje

cells, indicating a partial mislocalization of this protein in the null mice (white arrows, b). Scale is 100 μm. Data shown are mean ± SEM.